[AMERICAN JOURNAL OF SCIENCE, VOL. 317, JANUARY, 2017, P. 1–33, DOI 10.2475/01.2017.01]

American Journal of Science

JANUARY 2017

IMPACT OF THE NORTH AMERICAN MONSOON ON ISOTOPE PALEOALTIMETERS: IMPLICATIONS FOR THE PALEOALTIMETRY OF THE AMERICAN SOUTHWEST

ALEXIS LICHT*,**,†, JAY QUADE*, ANDREW KOWLER*,***, MARIE DE LOS SANTOS*,§, ADAM HUDSON*, ANDREW SCHAUER**, KATHARINE HUNTINGTON**, PETER COPELAND§, and TIMOTHY LAWTON§§

ABSTRACT. **Paleoaltimetric studies have characterized in detail the relationship between carbonate oxygen isotope ratios ($\delta^{18}O_c$) and elevation in orogens with simple, single-moisture-source hydrological systems, and applied this relationship to ancient continental carbonates to provide constraints on their past elevation. However, mixing of different atmospheric moisture sources in low-elevation orogens should affect $\delta^{18}O_c$ values, but this effect has not yet been confirmed unequivocally. In the American Southwest, summer monsoonal moisture, sourced in the Equatorial Pacific and the Gulf of Mexico, and winter moisture, sourced in the East Pacific, both contribute to annual rainfall. We present stable isotope results from Quaternary carbonates within the American Southwest to characterize the regional $\delta^{18}O_c$-elevation relationship. We then provide stable isotope results from local Eocene carbonates to reconstruct late Laramide paleoelevations.**

The Quaternary $\delta^{18}O_c$-elevation relationship in the American Southwest is not as straightforward as in more simple hydrological systems. $\delta^{18}O_c$ changes with altitude are non-linear, scattered, and display an apparent isotopic lapse rate inversion above 1200 m of elevation. We speculate that decreasing surface temperatures at high altitudes limit the duration of carbonate growth to the summer months, biasing $\delta^{18}O_c$ values toward higher values typical of the summer monsoon and leading to lapse rate inversion.

$\delta^{18}O_c$-elevation relationships based on modern water isotope data or distillation models predict paleoelevations that range up to as much as 2 km higher than the modern elevations of 2000 to 2400 m for our late Eocene sites located at the southern edge of the Colorado Plateau. By contrast, our $\delta^{18}O_c$-elevation relationship for the American Southwest yields lower paleoelevation estimates. These alternate estimates nonetheless suggest that significant elevation (at least ~1 km) had already been attained by the Eocene, but are also compatible with < 1 km of uplift by post-Laramide mechanisms. Our results show the limitations of standard $\delta^{18}O_c$-elevation models in complex hydrological systems and suggest that similar mechanisms may have led to summer-biased paleoaltimetry estimates for the initial stages of other orogenies —in the American Southwest and elsewhere.

Keywords: Paleoaltimetry, Colorado Plateau, Oxygen isotopes

INTRODUCTION

Recent studies using stable isotope paleoaltimetry have shown the efficacy of this method for estimating the paleoelevation of basins in western North America (for

* Department of Geosciences, University of Arizona, Tucson, Arizona USA
** Department of Earth and Space Sciences, University of Washington, Seattle, Washington USA
*** Department of Earth, Space, and Planetary Sciences, UCLA, Los Angeles, California USA
§ Department of Earth and Atmospheric Sciences, University of Houston, Texas USA
§§ Centro de Geociencias, Universidad Nacional Autónoma de México, Querétaro, México
† Corresponding author: licht@uw.edu

example, Mulch and others, 2007; Cassel and others, 2009; Hren and others, 2010; Mix and others, 2011; Lechler and others, 2013; Snell and others, 2014; Hough and others, 2014; Fan and others, 2014). Stable isotope paleoaltimetry is based on the decrease of the $\delta^{18}O$ and δD values of rainfall with increased elevation, in areas dominated by precipitation from a single moisture source (Poage and Chamberlain, 2001; Rowley and others, 2001). The relationship of $\delta^{18}O$ with altitude is calibrated by collecting rainfall or small, local discharge sources. Regional lapse rates vary between about −1.5 to - 2.9 ‰/km (Poage and Chamberlain, 2001; Blash and Bryson, 2007; Quade and others, 2011; Schemmel and others, 2013), in agreement with distillation models that predict isotope lapse rates in response to changing atmospheric relative humidity and temperature during orographic ascent (Rowley and others, 2001; Rowley, 2007; Rowley and Garzione, 2007; Mulch, 2016). This effect of altitude is archived in pedogenic carbonates by $\delta^{18}O_c$ values ($\delta^{18}O$ for carbonates, expressed in ‰ relative to the V-PDB standard). Pedogenic carbonates form as the soil dries after seasonal rainfall, occurring at different times of the year depending on local climates (Gallagher and Sheldon, 2016). This phenomenon is favored with increased soil temperatures during the warmer seasons because high soil temperatures increase the concentration of soil water and decrease calcium solubility through evaporation and plant evaporatranspiration (Breecker and others, 2009; Quade and others, 2013). Soil carbonate growth may not only be summer-biased, but also occur in extreme warm and dry events such as droughts that may occur at any time of year (Peters and others, 2013; Hough and others, 2014). Once these seasonal biases in soil water incorporation have been taken into account, $\delta^{18}O_c$ values can be used to estimate past $\delta^{18}O$ values of rainfall, and thereby infer paleoelevation (Kent-Corson and others, 2006, 2013; Chamberlain and others, 2012).

Stable isotope paleoaltimetry studies based on pedogenic carbonates have emphasized the importance of the Laramide orogeny (*ca.* 80–40 Ma) for mountain building in western North America and proposed near-modern elevation for the Sierra Nevada and Rocky Mountains in the late Eocene, and up to 2000 m higher than today for the proto-Basin and Range province, in the central and northern portions of the western U.S. (fig. 1A; Lechler and others, 2013; Snell and others, 2014; Hough and others, 2014). These results are also corroborated by other stable isotope paleoaltimetry archives, such as $\delta^{18}O$ of fossil mammal teeth and gastropods, δD analysis of clays, leaf waxes, and volcanic glass (Dettman and Lohmann, 2000; Fricke, 2003; Mulch and others, 2006, 2007; Fan and Dettman, 2009; Cassel and others, 2009; Hren and others, 2010). However, the timing of surface uplift for the Colorado Plateau and adjacent areas in the southwestern U.S. is still a matter of significant controversy (for example, Sahagian and others, 2002; Flowers and others, 2008; Huntington and others, 2010; Cather and others, 2012). Numerous studies have emphasized the importance of the post-Laramide (40–0 Ma) period for significant Colorado Plateau uplift, attributed to (1) the demise of the Farallon flat slab, or (2) epeirogenic uplift by convective removal of lithosphere or heating from below, associated with Basin and Range extension (Bird, 1979; Thompson and Zoback, 1979; Parsons and McCarthy, 1995; Spencer, 1996; Zandt and others, 2004; Roy and others, 2005; Moucha and others, 2009; van Wijk and others, 2010; Levander and others, 2011). All of these tectonic models suffer from inadequate information about the timing of surface uplift. Recent thermochronometric and stable isotope data from the central Colorado Plateau have been used to argue both in favor of (Karlstrom and others, 2014), and against (Huntington and others, 2010; Flowers and Farley, 2012) significant post-Miocene uplift. Precise paleoelevation estimates from the southern Colorado Plateau, its incised southern margin —the Mogollon Rim, and adjacent physiographic provinces in southern Arizona and New Mexico, are virtually non-existent, despite strong evidence that regional

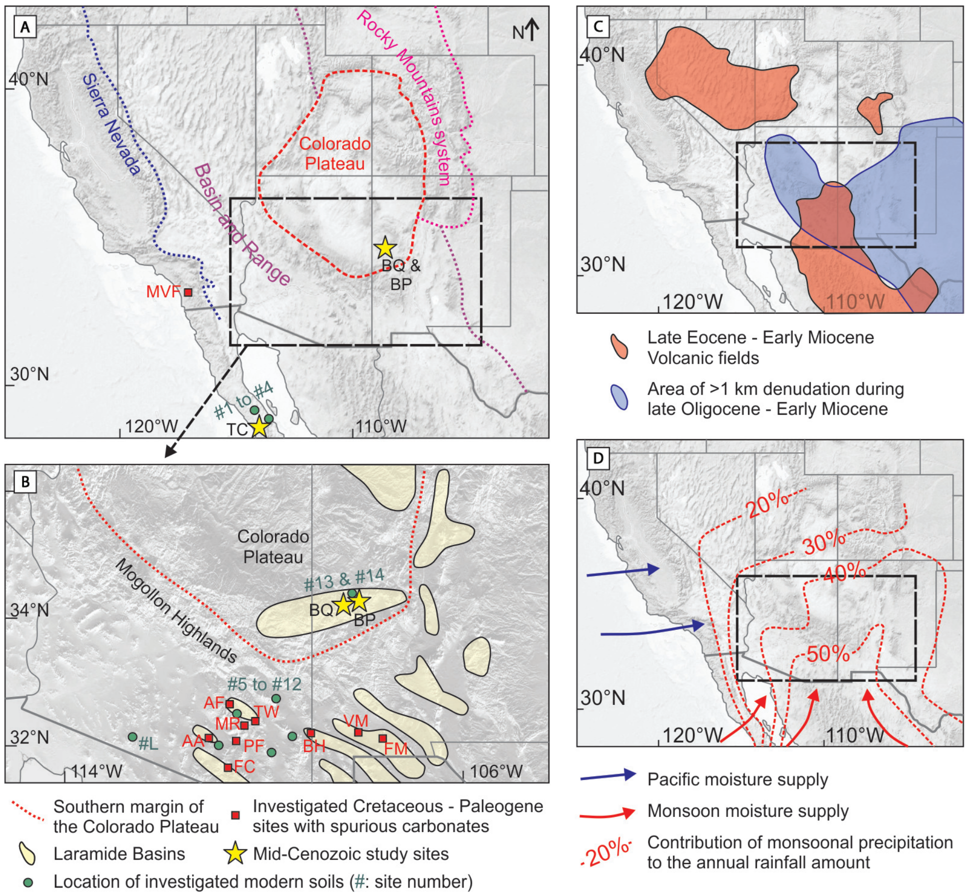

Fig. 1. (A, B): Map of the American Southwest with main structural provinces, Laramide basins (in yellow) and approximate location of the study sites. MVF: Mission Valley Formation; TC: Lomas Las Tetas de Cabras Formation; BQ: Baca Formation, Quemado section; BP: Baca Formation, Pie Town section; AF: American Flag Formation; MR: Mineta Formation, Mineta Ridge section; TW: Mineta Formation, Teran Wash section; AA: Amole Arkose; PF: Pantano Formation; FC: Fort Crittenden Formation; BH: Bobcat Hill Formation; VM: Lobo Formation, Vittorio Mountains section; FM: Lobo Formation, Florida Mountains section. #1 to #15 indicate the approximate location of sampled modern soils; #L indicates the location of the soils from Liu and others (1996). (C): Late Eocene and Oligocene volcanic fields and areas of significant denudation in the American Southwest; after Cather and others (2012). (D): Contribution of summer monsoonal rainfall (defined here as the sum of rainfall during July, August and September) to annual rainfall, highlighting the monsoonal domain; after Douglas and others (1993).

exhumation was particularly intense during the Laramide orogeny. From 80 to 40 Ma, the southern margin of the Colorado Plateau and numerous isolated ranges farther south were deeply eroded (commonly >1500 m) in response to uplift (Flowers and others, 2008). Moreover, evidence for significant denudation in the Oligocene – early Miocene, marked by deep regional erosion of >1000 m (fig. 1C), has been alternately suggested to reflect a major episode of increased mantle buoyancy associated with concurrent volcanism (Peirce and others, 1979; Cather and others, 2008, 2012) and drainage reversal along the Mogollon Rim (Flowers and others, 2008). The magnitude of surface uplift associated with either of these unroofing episodes is virtually unknown. South of the Mogollon Rim, potential Laramide and post-Laramide elevation gains have been significantly offset by subsidence and basin formation following

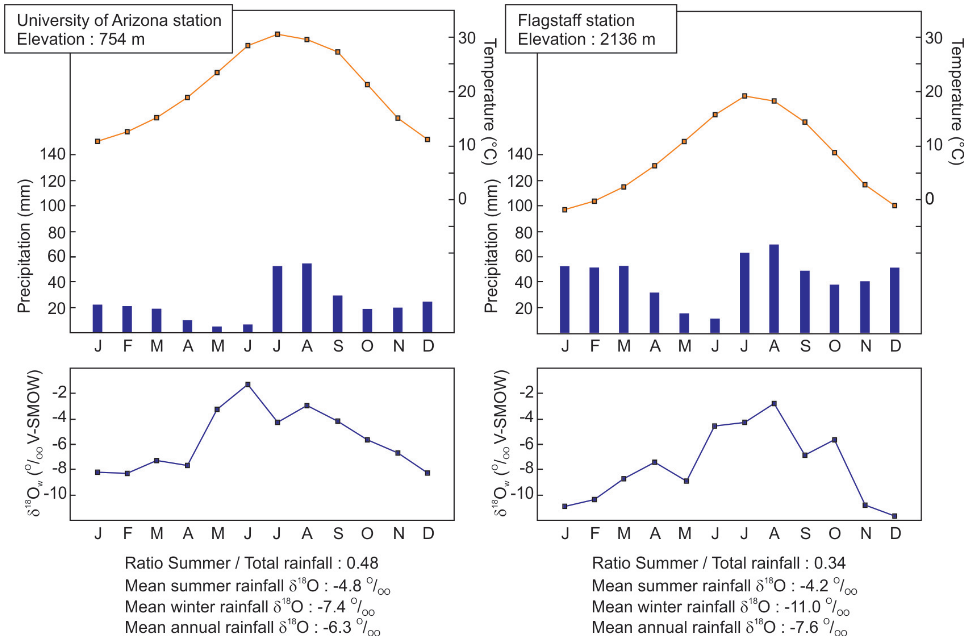

Fig. 2. Average monthly precipitation (mm), temperature (°C), rainfall $\delta^{18}O_w$, and mean summer, winter and annual rainfall $\delta^{18}O_w$ for two climatic stations in southern Arizona: University of Arizona station, Tucson (elevation 754 m) and Flagstaff (elevation 2140 m). Precipitation amount and temperature data from WRCC (2015); $\delta^{18}O$ data from Wright (ms, 2001), O'Brien and others (2006), and EIL (2015).

mid-Tertiary (Oligocene to mid-Miocene) fault-block extension associated with core complex uplift, and later Mio-Pliocene Basin-and-Range extension (Dickinson, 1991; Seager, 2004; Serkan-Arca and others, 2010).

Upper Cretaceous to Paleogene continental strata interpreted to record syn- and post-Laramide orogenesis are common and occupy local depocenters in the American Southwest (fig. 1B). These strata are commonly interfingered with and overlain by late and post-Laramide volcanic and volcaniclastic deposits, providing broad temporal control on the age of adjacent Laramide uplifts (for example, Seager and Mack, 1986; Inman, 1987; Lawton and others, 1993; Buck and Mack, 1995; González-León and Lawton, 1995; Seager, 2004; Copeland and others, 2011; Clinkscales and Lawton, 2015). Importantly, many of these basins contain pedogenic and lacustrine carbonates that are good targets for isotopic evaluation of paleoelevation.

However, the mixed character of modern rainfall in the American Southwest poses a major challenge to traditional approaches to paleoelevation reconstruction that employ simple isotope-elevation lapse rates. Most of the Sierra Nevada and Rocky Mountains are fed exclusively by East Pacific-sourced winter rainfall, whereas in the American Southwest, a significant part (often >30%) of annual rainfall is brought there by summer monsoonal storms sourced from the Gulf of California or the Gulf of Mexico (Douglas and others, 1993; fig. 1D). Summer monsoonal rainfall commonly displays higher $\delta^{18}O_w$ ($\delta^{18}O$ in water, in ‰ relative to V-SMOW standard) values than winter, East Pacific-sourced rainfall, showing a difference in rainfall $\delta^{18}O_w$ values of up to 9 permil between summer and winter (fig. 2; Wright and others, 2001; O'Brien and others, 2006; Blash and Bryson, 2007). Accordingly, the isotopic composition of continental carbonates in the American Southwest is likely to be affected by monsoonal moisture delivery and might be expected to display a different $\delta^{18}O_c$-elevation relationship than in other parts of the western USA where summer rainfall is slight.

As a first step toward understanding the impact of the monsoonal climate on carbonate isotopic values in southwestern North America, this study documents the isotopic values of late Quaternary pedogenic carbonates at various altitudes in the American Southwest in order to calibrate the $\delta^{18}O_c$-elevation relationship. We then apply this relationship to $\delta^{18}O_c$ values of mid-Cenozoic carbonates to document the late Laramide paleo-altimetry of the American Southwest.

BACKGROUND AND APPROACH

Physiography of the North American Monsoon

The inland domain of the North American monsoon extends over much of the western U.S., but the region where summer precipitation commonly exceeds 30 percent of the annual total is limited to the American Southwest (fig. 1D). Moist summer air masses entering the continental interior, sourced in the Gulfs of California and Mexico, are bound to the west by the peninsular ranges of southern California and Baja California, as well as the Sierra Nevada of central and northern California. The latter ranges also limit penetration of air masses from the East Pacific into the monsoonal domain (Douglas and others, 1993). Elevation generally increases but local relief is highly variable along the trajectory of summer moisture masses across the Southwest, from Baja California to the southern edge of the Colorado Plateau. The landscape ranges from mid-low altitude (0–1000 m) mountain ranges with high relief along the Baja California seashore, to mid-altitude (500–1200 m), flat basins in the Sonoran and southern Arizona Basin and Range province, to high-altitude (1000–3000 m), high-relief ranges in the Mogollon Rim, finally reaching the flat, high altitude (2000–2500 m) Colorado Plateau. Significant monsoonal moisture reaches the Mogollon Rim and the southern edge of the Colorado Plateau, where it is enhanced by orographic effects (Adams and Comrie, 1997). Areas located farther north of the Colorado Plateau generally receive less summer rainfall (<20 % of the annual rainfall). Summer rainfall contributes 30 to 50 percent of annual precipitation from the south edge of the Colorado Plateau southward across the Mogollon Rim (fig. 1D). $\delta^{18}O_w$ values of summer rainfall are commonly 2 to 9 permil higher than winter rainfall (Wright, ms, 2001; O'Brien and others, 2006; Blash and Bryson, 2007; fig. 2). Precipitation amount is highly sensitive to the local topography and increases with elevation; winter precipitation increases slightly more than summer precipitation with elevation gain, but varies locally. Wintertime rainfall from the East Pacific is associated with baroclinic systems that direct moist low-level flow against North America (James and Houze, 2005). In these simple weather systems, water isotope variations are well represented by standard distillation models for the evolution of rainfall isotopic composition with altitude, although the impact of terrain blocking on rainfall $\delta^{18}O_w$ is still debated (Poage and Chamberlain, 2001; Mulch and others, 2006; Galewsky, 2009). Summer monsoonal precipitation in the Southwest, on the other hand, is driven by atmospheric moist convection (Adams and Comrie, 1997). Effects of convective processes on rainfall isotopic composition result in the so-called 'amount effect' linking rainfall amount to rainfall depletion in ^{18}O and ^{2}H (Risi and others, 2008). In the American Southwest, the amount effect is hardly observable (Eastoe and Dettman, 2016) and it is unclear how it may change with altitude. Monitoring of rainfall isotopic compositions at different elevation sites shows that $\delta^{18}O_w$ lapse rates for both winter and summer seasons, and for the annual average, display a relatively robust linear trend, estimated at −2.6 ‰/km in the Mogollon Rim (elevation z > 1000m; Blasch and Bryson, 2007), close to the average isotopic lapse rate throughout the continental U.S. (−2.9 ‰/km; Dutton and others, 2005). We thus consider to a first-order approximation that both wintertime and summertime moisture follow similar distillation processes and isotopic lapse rates.

Compilation of Modern Pedogenic Carbonates

Modern soil carbonates were sampled along a topographic gradient ranging from 0 to 2500 m (fig. 1). All sites are located in the domain of the North American summer monsoon, in two main regions: sites near sea level are located in Baja California, Mexico (four sites), where locally sourced summer rainfall contributes 20 to 30 percent of annual precipitation, and sites above 700 m in Arizona and New Mexico (ten sites), where summer rainfall, sourced both in the Gulf of California and Gulf of Mexico, contributes 30 to 50 percent of annual precipitation (fig. 1B; Douglas and others, 1993). We confined our sampling to most-recent soils. Selected pedogenic carbonates were all exposed along fresh arroyo cuts, and their recent (likely Holocene) age was assessed from soil morphology, including the degree of development of calcic and cambic horizons (Gile and others, 1966; Quade and others, 2013). At each site, we sampled multiple exposures, where available, to take into account local $\delta^{18}O_c$ variability and at least six samples per site were analyzed for $\delta^{18}O_c$. All carbonates were sampled at least 50 cm below the soil surface (and commonly between 120 and 60 cm), in order to avoid evaporative isotopic bias in shallow soil waters (Quade and others, 1989; Breecker and others, 2009).

All carbonate samples were micro-drilled with drill bits 0.5 to 1 mm diameter at the University of Arizona, Tucson Arizona. $\delta^{18}O$ and $\delta^{13}C$ of carbonates were measured using an automated carbonate-preparation device (KIEL-III) coupled to a gas-source isotope ratio mass spectrometer (Finnigan MAT 252). Powdered samples were reacted with dehydrated phosphoric acid under vacuum at 70 °C. The isotope ratio measurement is calibrated based on repeated measurements of NBS-18 and NBS-19 and precision is $\pm$ 0.10 ‰ for $\delta^{18}O$ and $\pm$0.08 ‰ for $\delta^{13}C$ (1σ).

Approximate sampling site locations are shown on figures 1A and 1B. Sample descriptions, GPS coordinates, and detailed results are given in Appendix table A1. Although this manuscript focuses on $\delta^{18}O$ values, $\delta^{13}C$ values for all the samples are also provided in the Appendix. Additional details about soil profiles and sampling methods can be found in Kowler (ms, 2007). The discussion also includes $\delta^{18}O_c$ values from soil carbonates sampled in southern Arizona at elevation ~660 m published by Liu and others (1996; carbonates sampled 50 cm below the soil surface only).

Survey of Late Cretaceous to Oligocene Carbonates from the American Southwest

During the course of our study, we investigated a large array of Upper Cretaceous to Oligocene units in the Southwest from the Pacific coast to the Colorado Plateau to identify well-preserved primary carbonates for Laramide paleoelevation reconstruction. Carbonate samples were prepared in thin sections and checked for carbonate texture. We then analyzed their isotopic composition following similar protocols as for modern carbonates. We also complemented our investigations by clumped-isotope analyses to further assess how our investigated carbonates have been altered (Huntington and others, 2011; Bristow and others, 2011; Henkes and others, 2015; Huntington and Lechler, 2015; Huntington and others, 2015). Clumped-isotope paleothermometry is based on the temperature dependence of the statistical overabundance of bonds between carbon ^{13}C and oxygen ^{18}O isotopes in carbonate minerals. The amount of $^{13}C^{18}O^{16}O$ relative to $^{12}C^{16}O_2$ in carbonates in excess of a random distribution is solely dependent upon temperature, and carbonate clumped-isotope analyses independently constrain carbonate formation temperature and $\delta^{18}O_c$.

Unfortunately, only a fraction of the data from the Cretaceous-Paleogene investigated sites were useable for paleoaltimetry reconstruction. Evidence of coarse-grained (>10–20 μm) microspar in the investigated carbonates showed that most samples collected were at least partially recrystallized; unrealistic $\delta^{18}O_c$ values (<-10 ‰ for coastal sites, <-17% for inland sites) highlighted a strong diagenetic overprint (table 1; Knauth and Kennedy, 2009; Boggs, 2009). Moreover, most of all clumped isotope temperatures obtained from the investigated units were markedly too high (>40 °C) to be considered reasonable for carbonate mineralization in lacustrine or pedogenic environments, and thus likely reflect diagenetic overprinting (Huntington and others, 2011; Passey and Henkes, 2012; Quade and others, 2013), either by secondary carbonate mineralization and/or partial thermal resetting due to chemical bond reordering at elevated temperature (Huntington and others, 2015). The scarcity of well-preserved, pre-Basin-and-Range primary carbonates in the American Southwest, despite the presence of numerous Laramide and post-Laramide sedimentary basins, is particularly noteworthy considering shallow burial depths and the lack of significant tectonic deformation. Elimination of these factors thus points to hydrothermal alteration rather than burial- or thrusting-related heating and diagenesis (Quade and others, 2013). Widespread Oligocene-Early Miocene magmatism in the American Southwest (Shafiqullah and others, 1978; Cather and others, 2012) and associated high crustal temperature gradients (Dickinson, 1991) are likely causes of the significant diagenetic imprint observed for pre-Basin-and-Range carbonates. We present all $\delta^{18}O_c$ values for all the investigated sites in Appendix table A2, and clumped isotope methodology and results are given in Appendix table A3.

For discussion purposes, we narrowed our focus to two Eocene units that appear to preserve primary isotopic values: the Eocene Baca Formation in south-central New Mexico and the Lomas Las Tetas de Cabra (LLTC) Formation in Baja California (fig. 1). Carbonates from these sections are purely micritic and display reasonable surface-like $\delta^{18}O_c$ (>-10 ‰ for coastal sites, >-17% for inland sites) and clumped-isotope temperature (<40 °C), $\delta^{18}O_c$ values from the Baca Formation should allow us to reconstruct its paleoelevation at the time of deposition. The LLTC Formation has always resided near sea level and therefore its $\delta^{18}O_c$ values provide key constraints on differences between Eocene and modern $\delta^{18}O_w$ values near sea-level.

Geological Context of the Selected Eocene Sites

The upper Eocene Baca Formation, Baca Basin, New Mexico.—The Baca Basin is a late Laramide-age basin surrounded by isolated uplifts following a roughly East-West trend, and extends over 300 km on the Colorado Plateau, from eastern Arizona to western New Mexico (Cather and Johnson, 1984). The deposits of the Baca Basin consist mainly of middle Eocene siliciclastic rocks (Baca Formation and Mogollon Rim Gravels) overlain by a thin cover (<300 m) of late Eocene - Oligocene volcaniclastic and volcanic rocks (Spears Formation; Prothero and others, 2004).

The Baca Formation in western New Mexico comprises fluvio-lacustrine sediments deposited by an east-flowing river system that drained the southern part of the Colorado Plateau and flowed down the Mogollon Rim during the Eocene (Cather and Johnson, 1984; Cather and others, 2012). The Baca Formation is dominated by fanglomerates to the west, by channel bodies and alluvial mudstones in its middle part, and by lacustrine mudstones to the east (Cather and Johnson, 1984). Alluvial facies of the Baca Formation have yielded numerous vertebrate remains of Duchesnean land mammal age (Lucas, 1983); magnetostratigraphic dating of a section near Quemado (Prothero and others, 2004) suggests a correlation with the base of Chron Cr17 (~38.5 – 38 Ma).

We investigated two sections of the Baca Formation. The first section, located in the Sawtooth Mountains north of Pie Town, is ~70 m thick and dominated by fine-grained alluvial deposits, in which we identified at least six paleosols containing stage I-II carbonates (*sensu* Gile and others, 1966). The second section is located north of Quemado, near Mariana Mesa, a section dated by magnetostratigraphy by Prothero

TABLE 1

Age, $\delta^{18}O_c$ values, carbonate texture, and clumped-isotope temperatures of investigated Laramide units for samples rejected in study

Unit	Location	Age	Reference	Material	$\delta^{18}O_c$ range (in ‰ V-PDB)	Carbonate texture	Clumped isotope temperature
American Flag Formation	San Pedro Valley, Arizona	Late Cretaceous	Dickinson (1991)	Conglomerate with calcite matrix and carbonate clasts	-10 to -17	Coarse, sparitic	-
Fort Crittenden Formation	Santa Rita Mountains, Arizona	Late Cretaceous	Inman (1987)	Pedogenic nodules, bivalves, gastropods, cements	-12 to -18	coarse, sparitic, rich in calcite veins; nodules sometimes septarian	-
Amole Arkose	Tucson Mountains, Arizona	Late Cretaceous	Lucas and others (2005)	Stromatolitic limestones	-12 to -16	Sparitic	-
Lobo Formation, Florida section	Florida Mountains, New Mexico	Paleocene – Early Eocene	Amato (2000)	Pedogenic nodules, lacustrine limestone, cements	-12 to -18	Sparitic, rich in calcite veins	164 to 228°C
Lobo Formation, Victorio section	Victorio Mountains, New Mexico	Paleocene – Early Eocene	Amato (2000)	Pedogenic nodules ?	-17 to -18	Sparitic, rich in calcite veins	-
Mission Valley Formation	San Diego, California	Late Eocene	Walsh and others (1996)	Pedogenic nodules	-11 to -12	Sparitic	-
Frias Formation	San Diego, California	Late Eocene	Walsh and others (1996)	Pedogenic nodules	-10 to -11	Sparitic	-
Bobcat Hill Formation	Peloncillo Mountains, Arizona	Eocene	Bayona and Lawton (2003)	Cement, lacustrine limestone?	none	Coarse, sparitic	-
Mineta Formation, Mineta Ridge section	San Pedro Valley, Arizona	Oligocene	Clay (1970)	Stromatolitic & oncolithic limestones, marls	-7 to -22	Sparitic, rich in calcite veins, sometimes partly silicified	93 to 145°C
Mineta Formation, Teran Wash section	San Pedro Valley, Arizona	Oligocene	Grover (1984)	Stromatolitic & oncolithic limestones, marls	-4 to -11	Sparitic, rich in calcite veins	45 to 58°C
Pantano Formation	Tucson Basin, Arizona	Oligocene	Grimm (1978)	Oncolithic limestones, marls	-7 to -12	Sparitic, rich in calcite veins	25 to 105°C

Location on figure 1. Detailed results and GPS coordinates in Supplementary Tables 2 and 3.

and others (2004). This section is ~90 m thick and is also fluvial with carbonate-bearing paleosols. Both field sites are today located between 2200 and 2400 m of elevation. Detailed maps of the study area are available in Prothero and others (2004) and Cather and Johnson (1984).

The Eocene Lomas Las Tetas de Cabra (LLTC) Formation, Baja California, Mexico.—The Eocene LLTC Formation is one of the few non-marine Paleogene units in the Mexican section of the Californian forearc basin, and crops out in central Baja California. Today, this unit lies at the margin of the American monsoonal realm and receives 20 to 30 percent summer rainfall (Novacek and others, 1991). Paleogeographical reconstructions taking into account the recent (Neogene) northward drift of Baja California Peninsula indicate that the LLTC Formation was likely located ~200 to 300 km further south at the time of deposition (McQuarrie and Wernicke, 2005), where today summer precipitation exceeds 50 percent of annual rainfall.

The LLTC Formation is dominated by continental rocks consisting of conglomeratic to sandy channel bodies and fine-grained, paleosol-bearing alluvial deposits (Flynn and others, 1989). It has yielded abundant mammalian fauna of Wasatchian (Early Eocene) land mammal age, and interfingers with rare mollusca- and foraminifera-bearing shallow marine strata (Novacek and others, 1991). Magnetostratigraphic dating of several sections suggests correlations with the end of Chron C24 or the base of Chron C23, between ~53.5 and ~51.5 Ma (Flynn and others, 1989).

We investigated and sampled the type section of the LLTC Formation, near LLTC Hill at a modern elevation of ~100 m (detailed map and section in Flynn and others, 1989). The section is ~90 m thick and dominated by fine-grained alluvial deposits, in which at least five, stage-I to stage-III carbonate-bearing paleosols were identified and sampled.

RESULTS

Modern Soils

$\delta^{18}O_c$ values from fourteen different soils and involving nearly 190 analyses range from −10.6 ‰ to −1.2 permil. When taken together, the $\delta^{18}O_c$ values are scattered and do not show any clear linear trend with elevation gain (fig. 3). Using a regression of average $\delta^{18}O_c$ values per locality, $\delta^{18}O_c$ values decrease from near sea-level values with an estimated lapse rate of −1.5 ‰ per 1000 m gain, but with low correlation coefficient (mean $\delta^{18}O_c = -1.5*10^{-3}z - 4.7$ for z between 0 and 2500 m, $r^2 = 0.29$).

Modern soil carbonates from Baja California display $\delta^{18}O_c$ values ranging from −6.3 to −1.2 permil, with site averages of −5.0 permil (site 1, elevation 65 m), −4.1 permil (Site 2, elevation 130 m), −5.4 permil (site 3, elevation 278 m), and −2.0 permil (site 4, elevation 670 m). $\delta^{18}O_c$ values from sites ranging from 600 m to 1600 m in Arizona and New Mexico decrease with elevation, from values similar to those from Baja California at low elevation (Site 5, elevation 710 m, $\delta^{18}O_c$ −5.8 to −2.7 ‰, average −3.9 ‰) to much lower values between 1200 m (site 8, elevation 1229 m, $\delta^{18}O_c$ −10.0 to −8.9 ‰, average −9.4 ‰) and 1600 m (site 10, elevation 1523 m, $\delta^{18}O_c$ −10.6 to −5.3 ‰, average −8.7 ‰). $\delta^{18}O_c$ variation with elevation between 0 to 1600 m visually follows the $\delta^{18}O_c$ - elevation regression curve of Quade and others (1989) for pedogenic carbonates in the Mojave desert, Nevada (located outside of the monsoonal realm), which predicts a decrease of −3.7 ‰ per 1000 m elevation gain. Using a regression through station mean $\delta^{18}O_c$ values, the lapse rate below 1600 m is estimated at −3.4 ‰ per 1000 m gain (mean $\delta^{18}O_c = -3.4*10^{-3}z - 3.4$, for elevation $z < 1600$ m, $r^2 = 0.53$). The correlation coefficient is much more robust if the highest values in the data set from stations #4 and #5 are excluded ($\delta^{18}O_c = -3.1*10^{-3}z - 3.3$, $r^2 = 0.85$). Intense evaporation at sites #4 and #5 relative to other sites may explain why

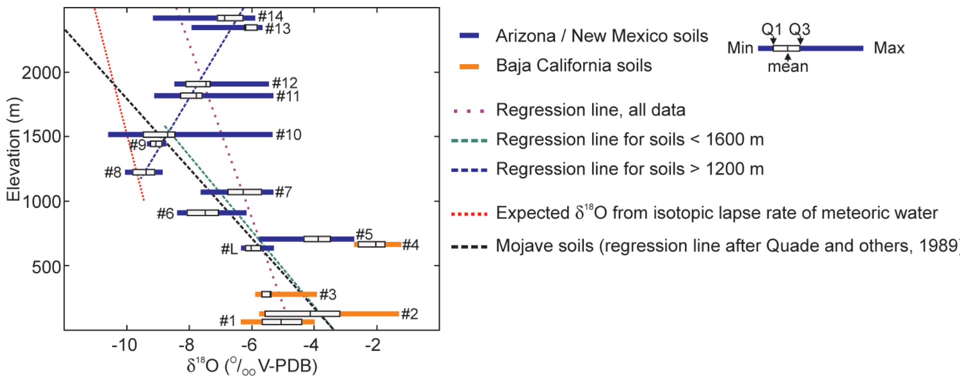

Fig. 3. Variations of $\delta^{18}O_c$ values of pedogenic carbonate in modern soils of Arizona, New Mexico (in blue) and Baja California (in orange). Boxes indicate lower (Q1) and upper (Q3) quartiles; inside boxes, solid lines indicate mean; whiskers indicate minimum and maximum values. #1 to #15 indicate our sample locality numbers; #L indicates soil values from the study of Liu and others (1996) in southern Arizona. Regression lines for mean $\delta^{18}O_c$ per locality (purple dotted line, mean $\delta^{18}O_c = -1.5*10^{-3}z - 4.7$), for mean $\delta^{18}O_c$ in soils < 1600 m (green dashed line, mean $\delta^{18}O_c = -3.4*10^{-3}z - 3.4$) and > 1200 m (blue dashed line, mean $\delta^{18}O = 2.5*10^{-3}z - 12.5$), for $\delta^{18}O$ in soils of the Mojave Desert, Nevada (black dashed line, after Quade and others, 1989), and expected $\delta^{18}O$ values for soil carbonates (red dashed line) calculated from the isotopic lapse rate of meteoric water from Blash and Bryson (2007), using the T-$\delta^{18}O$ equation of Kim and O'Neil (1997), MAT + 8 °C for temperature of soil carbonate growth (Quade and others, 2013), and the relation MAT = − 0.0069*z+24.62 (r^2 = 0.95) calculated from 15 climatic stations in southern Arizona (WRCC, 2015). Detailed results in Appendix table A1.

these $\delta^{18}O_c$ values are higher than expected (Quade and others, 1989; Breecker and others, 2009).

In contrast, sites located above 1200 to 1600 m follow a significantly different pattern compared to the Mojave regression curve. $\delta^{18}O_c$ values are relatively constant between 1200 and 1600 m and then follow a slight but statistically robust increasing trend of +2.5 ‰ per 1000 m (mean $\delta^{18}O_c = 2.5*10^{-3}z - 12.5$ for elevation z >1200 m, $r^2 = 0.94$), with maximum values reached at the two sites located in the Colorado Plateau (site 13, elevation 2348 m, average −6.2 ‰, and site 14, elevation 2425 m, average −6.8 ‰).

There is no clear trend of $\delta^{18}O_c$ variation with latitude, longitude or distance to the Pacific (not shown). This is illustrated by the close similarities between $\delta^{18}O_c$ values at site #3 in Baja California and at site #5, located 460 km northeastward in southern Arizona. In contrast, mean $\delta^{18}O_c$ at site #9 (elevation 1451 m) is lower by 5.2 permil than at site 5 (elevation 710 m), whereas both sites are only 20 km distant to each other.

Ancient Soil Carbonates

Discrete carbonate nodules from Baca and LLTC Formations are made up of sub-hedral micrite, with rare, coarser crystalline microspar calcite (grain diameter >4 μm) limited to small veins and fracture-filling cement, suggesting good preservation of primary carbonate (Deutz and others, 2002; Boogs, 2009). $\delta^{18}O_c$ values for both units are all >−15 permil (table 2). Additionally, clumped-isotope analyses were performed on the Baca Formation, including three to four replicates per sample to ensure good reproducibility of the clumped-isotope values (Huntington and Lechler, 2015). Estimated clumped-isotope temperatures ranged from 25 to 58 °C, with at least three samples with plausible surface-like values (25 °C and 36 °C twice). The primary character of the micrite and the relatively narrow range of temperatures in Baca Formation samples strongly suggest partial solid-state temperature resetting (instead of secondary carbonate recrystallization) as the dominant cause for the few high

TABLE 2

$\delta^{18}O_c$ value ranges of Eocene limestones used in this study

	Locality / Unit	Reference	Material	$\delta^{18}O_c$ range (in ‰ V-PDB)
Eocene alluvial units	Baca Fm (Southern Colorado Plateau, New Mexico), Late Eocene	Prothero and others (2004)	Pedogenic nodules (n=24)	-8.5 to -12.4, average -10.1
	LLTC Fm (Baja California), Early Eocene (near sea level station)	Flynn and others (1989)	Pedogenic nodules (n=16)	-7.2 to -0.3, average -5.1

Location on figure 1. Detailed results in Supplementary Table 2.

clumped-isotope temperatures, indicating that primary $\delta^{18}O_c$ values have been preserved (Huntington and Lechler, 2015; Huntington and others, 2015). Although we did not supplement thin section observations and $\delta^{18}O_c$ analyses for the LLTC Formation with clumped-isotope analyses, pairing of these proxies suggests that $\delta^{18}O_c$ can be considered primary in this sample suite as well.

$\delta^{18}O_c$ values from pedogenic nodules of the LLTC Formation are similar to those of Quaternary carbonates from Baja California and range from −7.2 to −0.3 permil (average −5.1 ‰). $\delta^{18}O_c$ values from the Baca Formation are ~5 permil lower and range from −12.4 to −8.5 permil (average −10.1 ‰). These values are also lower than modern $\delta^{18}O_c$ values in the vicinity. Modern values below −10 permil similar to those of the Baca Formation are only found between 1200 and 1600 m (sites #8 and #10), although average values at these elevations are slightly higher (−8.7 to −9.4 ‰).

OXYGEN ISOTOPE-BASED PALEOALTIMETRY IN THE AMERICAN SOUTHWEST

Mechanisms for the Modern $\delta^{18}O_c$-Elevation Relationship in the North American Monsoonal Domain

Our data from Quaternary soil carbonates are particularly scattered and do not show a well-defined trend toward lower $\delta^{18}O_c$ values with elevation increase, in contrast to regions receiving a single moisture source (Quade and others, 1989, 2007a, 2011; Rowley and others, 2001).

For comparison, the mean annual $\delta^{18}O_w$ value of meteoric water in the Mogollon Rim (z > 1000 m) from Blash and Bryson (2007) can be used to predict soil carbonate $\delta^{18}O_c$ values following the temperature-dependent fractionation relationship of Kim and O'Neil (1997). We assume Mean Annual Temperature (MAT) + 8 °C at soil depth (Quade and others, 2013) and a MAT - elevation linear relationship based on climatic station data in southern Arizona, with a decrease of 6.9 °C per 1000 m gain (see fig. 3). Predicted $\delta^{18}O_c$ values decrease by −1.1 permil per 1000 m gain (fig. 3, dashed red line); this lapse rate is close to the poorly constrained lapse rate of −1.5 ‰/km observed among all modern soil localities. However, most observed $\delta^{18}O_c$ values exceed predicted $\delta^{18}O_c$ values, and the trend toward lower $\delta^{18}O_c$ values with elevation gain is only poorly defined, with low correlation coefficient and many localities falling completely outside the regression bounds.

The behavior of soil $\delta^{18}O_c$ values below 1600 m, although scattered, mirrors the $\delta^{18}O_c$-elevation relationship found in the nearby Mojave Desert, where soil evaporation is the dominant control on $\delta^{18}O_c$ values (Quade and others, 1989). Under arid conditions, evaporation in soils can significantly enrich in soil pore waters in ^{18}O, the intensity of which decreases with increasing altitude (Quade and others, 1989, 2007a, 2007b). Considering the extreme aridity of southern Arizona and Baja California, it is not surprising that the $\delta^{18}O_c$-elevation relationship at low altitude resembles the regression curve found in the Mojave Desert. High values at sites #4 and #5, falling outside the regression bounds, suggest that other factors may have locally emphasized evaporation effects, such as soil texture, soil maturity, or vegetation cover (Liu and others, 1996; Breecker and others, 2009).

The increase of soil $\delta^{18}O_c$ values above the 1200 to 1600 m threshold is a trend not previously documented along altitudinal transects and cannot be explained by changes in evaporation or in seasonal rainfall contribution with altitude. Evaporation would tend to decrease at high elevation, resulting in lower $\delta^{18}O_c$ values. Moreover, a decreased ratio of summer:annual rainfall with altitude gain would also result in lower $\delta^{18}O_c$ due to an increased contribution from ^{18}O-depleted winter precipitation (fig. 2).

Seasonality of soil carbonate growth may explain why $\delta^{18}O_c$ values >1200 to 1600m increase with elevation and thus deviate from expectation. At low altitude (<1000 m) in the American Southwest, temperature is relatively high all year long. For example, monthly temperature exceeds 10 °C during the whole year in Tucson (fig. 2A). Consistently high annual temperatures predict that episodic, minor carbonate growth is likely to occur following each rain event regardless of season, thus mixing the oxygen isotopic signals of winter and summer rainwater. Monitoring of soil water $\delta^{18}O_w$ and pedogenic $\delta^{18}O_c$ values at the same low altitude (~640 m high) site in southern Arizona by Liu and others (1995, 1996) suggests that carbonate growth incorporates oxygen from seasonally mixed water, although partly biased toward the late spring and early summer period preceding the monsoon season, when evapotranspiration is highest. By contrast, carbonate growth at high altitude outside the peak summer season is highly improbable due to low cool season (fall to spring) temperatures, diminishing evaporation and thus carbonate formation. For instance, at 2100 m monthly air temperatures exceed 10 °C only from May to September (fig. 2B). Clumped-isotope temperatures from two soils at high elevation (>1000 m) in southern Arizona corroborate such a mid-summer bias in carbonate growth (Quade and others, 2013), whereas this summer bias is absent in two other soils at lower elevation (<1000 m; Gallagher and Sheldon, 2016). This bias towards summer rainfall events should result in higher $\delta^{18}O_c$ values reflecting increased contribution from monsoon-derived, and therefore ^{18}O-enriched, meteoric water. This simple bias alone can account for the scattering and the apparent increase in $\delta^{18}O_c$ values with elevation above 1200 to 1600 m. Hence, we propose a dual mechanism to explain the observed $\delta^{18}O_c$-elevation relationship for carbonates in the North American monsoonal domain (fig. 4A):

(1) below 1200 to 1600 m of elevation, carbonate growth occurs after rainy events throughout most of the year with a potential bias toward late spring/early summer, but $\delta^{18}O_c$ values are mainly controlled by evaporation of winter/spring soil water, leading to a scattered decrease in $\delta^{18}O_c$ values with elevation gain in this low elevation zone (for example, Quade and others, 2007a);

(2) above 1200 to 1600 m, decreasing temperature limits the period of strong evaporation and carbonate growth to a reduced interval during the summer, and $\delta^{18}O_c$ values are higher due to incorporation of a higher proportion of monsoonal soil water. Amount of ^{18}O enrichment increases as the length of the favorable season is reduced toward summer, leading to $\delta^{18}O_c$ increase with elevation gain. This pattern should persist until $\delta^{18}O_c$ values converge on the expected $\delta^{18}O_c$ values calculated from summer rainfall $\delta^{18}O_w$ only. Unfortunately, this convergence is undocumented in our dataset due to the lack of carbonate nodules in soils at higher altitudes than 2500 m

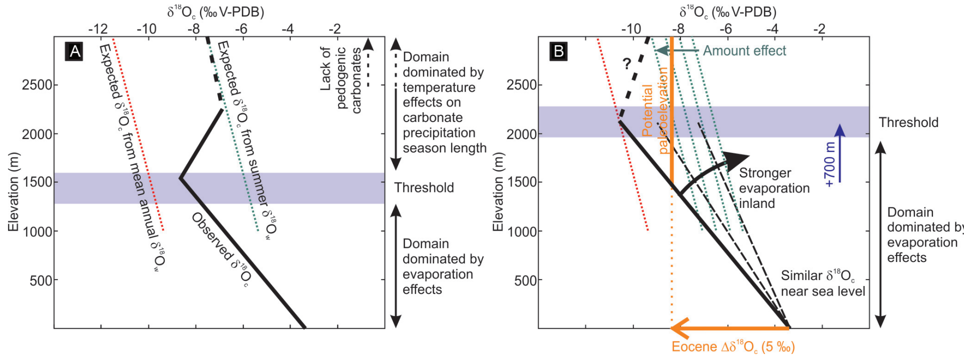

Fig. 4. (A) Model for modern pedogenic carbonate $\delta^{18}O_c$ variation with elevation gain (black line), compared with expected $\delta^{18}O_c$ variation calculated from mean annual $\delta^{18}O_w$ values (see also fig. 3, red dashed line) and from mean summer $\delta^{18}O_w$ values (green dashed line; considering a −4 ‰ difference between mean annual and summer $\delta^{18}O_w$ values, similar to that observed near Flagstaff, fig. 2). (B) Modeled Eocene conditions of higher temperature and evaporation on the $\delta^{18}O_c$-elevation relationship. Expected $\delta^{18}O_c$ variation calculated from mean annual $\delta^{18}O_w$ values (red dashed line) remains unchanged but behavior threshold is shifted by 700 m, corresponding to the impact of a gain of 5 °C; expected $\delta^{18}O_c$ variation calculated from summer $\delta^{18}O_w$ values (green dashed lines) is shifted to lower values as a response to a potential increase of monsoonal amount effect (see main text). Whereas coastal $\delta^{18}O_c$ values remain unchanged, inland lapse rate can be potentially modified due to stronger evaporation inland. Range of potential paleoelevations for the Baca Formation, calculated using $\Delta\delta^{18}O_c$= 5.0 ‰, is shown in orange.

within the study area, which is also noted in the Mojave Desert region (Quade and others, 1989).

Implications for Paleoaltimetry Studies

Meaningful and precise paleoelevation estimates in the American Southwest based on the isotopic $\delta^{18}O_c$-elevation relationship outlined previously are difficult to determine, particularly above 1200 m, where the scattering of data and an apparent reversed lapse rate confound interpretation of stable isotope data with respect to distinguishing high from low (<1200 m) elevations. Moreover, the significant role of monsoonal rainfall in shaping the $\delta^{18}O_c$-elevation relationship raises questions about its longevity through time, considering the high monsoonal variability on millenial (Poore and others, 2005) and longer time scales (Sewall and Sloan, 2006; Fricke and others, 2010). Past lapse rates in non-evaporative, single-sourced precipitation systems can be evaluated by adjusting rainfall $\delta^{18}O_w$ near sea level and adiabatic lapse rates (Rowley and others, 2001; Rowley and Garzione, 2007). In contrast, the past $\delta^{18}O_c$-elevation relationship in the American Southwest is complex and must take into account at least three distinct phenomena, as follows.

First, changes in mean annual rainfall $\delta^{18}O_w$ would shift the $\delta^{18}O_c$-elevation relationship, but the amplitude of this shift can be quantified by comparing $\delta^{18}O_c$ values in modern and past near-sea level sites at the same location, as for single sourced systems (Rowley and others, 2007; Quade and others, 2007a, 2011). However, different $\delta^{18}O_w$ values of summer monsoonal rainfall, which are much harder to quantify in the fossil record, could affect the $\delta^{18}O_c$-elevation relationship above some elevation threshold marking the shift from the lower elevation, evaporation intensity-controlled negative lapse rate to the higher elevation, summer temperature-controlled positive lapse rate (fig. 3). Lower (higher) summer $\delta^{18}O_w$ would decrease (increase) the gain of $\delta^{18}O_c$ values with altitude above this threshold. A more intense amount effect on summer precipitation due to stronger monsoonal convection could have, in the past, changed the relationship above the 1200 to 1600 m threshold.

Second, regional changes in annual (or seasonal) temperatures should impact the altitude of the negative-positive lapse rate threshold. For example, higher fall and spring temperatures at high altitude would extend the length of the carbonate growth season into fall and spring, whereas lower temperatures would reduce it. Considering the modern temperature-elevation relationship in the American Southwest (fig. 3), a regional +1°C increase in annual temperature would increase the altitude of the threshold by approximately 140 m.

Finally, changes in aridity in the American Southwest and modifications of the evaporation/precipitation balance should significantly impact the lapse rate below the threshold, where evaporation effects –rather than changes in rainfall $\delta^{18}O_w$– control $\delta^{18}O_c$ values (Quade and others, 2007a). This impact is expected to be particularly strong during drier periods in the American Southwest and should result in ^{18}O-enrichment at low altitude.

Based on the complexity of soil carbonate formation in a mixed climate such as modern Arizona, the prognosis for precise paleoelevation estimates is poor, as it requires a large number of assumptions about past hydrological parameters and temperatures. Basic considerations of the Eocene climate allow a very coarse estimate of changes in the behavior of the $\delta^{18}O_c$-elevation relationship in the past. However, the reader should keep in mind that the estimates given in the following section are primarily qualitative, rather than quantitative, due to the above complications.

APPLICATION TO MID-CENOZOIC PALEOALTIMETRY AT THE SOUTHERN EDGE OF THE COLORADO PLATEAU

Paleoaltimetry estimates based on measured or modeled lapse rates require a knowledge of the $\delta^{18}O_c$ values from near-sea level at the time in question. Finding coeval near-sea level sites is particularly difficult in deep-time, when the stratigraphic record is less complete and precise. Paleoaltimetry studies do not commonly provide near-sea level paleo-data but rather make assumptions about what the near sea level values should be (for example, Rowley and Curie, 2006; Mix and others, 2011; Hoke and others, 2014; Ding and others, 2014). Here, we propose to use LLTC Formation values as a proxy for Eocene $\delta^{18}O_c$ values from near-sea level. Mean $\delta^{18}O_c$ values (−5.1 ‰) from the LLTC Formation are very similar to the range of $\delta^{18}O_c$ values in the modern soils near sea level (−4.8 ‰ on average for the three stations below 300 m of elevation). The expected −1 permil shift in isotopic composition due to the impact of early Eocene ice-free conditions on the global hydrologic cycle (for example, Tindall and others, 2010) is here poorly expressed; this lack of expression is, however, in agreement with the regional seawater oxygen isotopic composition simulations of Tindall and others (2010), which show that early Eocene seawater $\delta^{18}O_w$ values along Californian shorelines were quasi-similar to those of today. More surprisingly, higher temperatures by 5 to 10 °C in early Eocene North America (Greenwood and Wing, 1995; Fricke and Wing, 2004; Hren and others, 2010) should have decreased the pedogenic $\delta^{18}O_c$ values by −1 to −2 permil, following the temperature-dependent fractionation relationship of Kim and O'Neil (1997). The lower predicted $\delta^{18}O_c$ values may have been counterbalanced by evaporative enrichment of ^{18}O in soil water. The range of Baja California $\delta^{18}O_c$ values similar to modern values there suggests that the extreme, ice-free greenhouse conditions of the early Eocene did not significantly impact coastal soil $\delta^{18}O_c$ values. This impact should be even less significant in the less extreme greenhouse conditions of the late Eocene (Pagani and others, 2005). Thus, although LLTC and Baca deposits are not coeval (LLTC older by ~12 – 14 Ma), we argue that the LLTC $\delta^{18}O_c$ data set is a suitable reference for late Eocene coastal conditions.

$\delta^{18}O_c$ values from the Baca Formation (average −10.1‰, but up to −12.4 ‰) are much lower than those found in modern soils at the current elevation between 2000 m

Table 3

Paleoelevation estimates for the Baca Formation

	Regression from modern precipitation data (predicted lapse rate : 1.1 ‰/km)	Distillation model	Regression for evaporative domain (lapse rate 1: 3.1 ‰/km) (lapse rate 2: 3.4 ‰/km)
Paleoelevation estimates for Baca Fm	4545 m ± 2273 m	3880 m +778/-1064 m	(1) 1471 m ± 806 m (2) 1613 m ± 735 m

Linear regression estimate from modern precipitation data (predicted lapse rate of 1.1 ‰/km) is calculated from $d^{18}O_w$ of meteoric water in the Mogollon Rim (Blash and Bryson, 2007), using $\Delta^{18}O_c$ = 5.0 ± 2.5 ‰ (1σ). Distillation model estimate is from the equations of Rowley (2007). Linear regression estimates for the evaporative domain are from the observed lapse rates given in section titled: Mechanisms for the modern $\delta^{18}O_c$-elevation relationship in the North American monsoonal domain. Errors (1σ) for regression estimates are those associated with the uncertainty in $\Delta^{18}O_c$ value (2.5 ‰). Errors for the distillation model are those associated with the uncertainty in carbonate growth temperature temperatures at both sites (see main text); they do not take into account the additional uncertainty associated with unknown mean starting temperature and relative humidity of air masses (+675/−844 m (1σ) at this altitude; Rowley, 2007).

and 2400 m in central Mogollon rim area: values below −10 permil are only found between 1200 and 1600 m.

We can merge our results from Eocene soil carbonates to estimate the paleoelevation of the Baca Formation on the modern Mogollon Rim (table 3). A $\Delta\delta^{18}O_c$ (mean $\delta^{18}O_c$ of Baca Formation samples minus mean $\delta^{18}O_c$ of LLTC Formation samples) of 5.0 ± 2.5 ‰ (1σ), and a predicted lapse rate of 1.1 ‰/km calculated from modern $\delta^{18}O_w$ of meteoric water in the Mogollon Rim (Blash and Bryson, 2007) yield a paleoelevation estimate of 4545 m ± 2273 m for the Baca Basin. Estimating paleoelevation with distillation models requires an estimate for the $\Delta\delta^{18}O_w$ (similar to $\Delta\delta^{18}O_c$ but for $\delta^{18}O_w$; Rowley and others, 2001). It can be calculated from mean $\delta^{18}O_c$ values from both units and estimates of carbonate growth temperatures using the T-$\delta^{18}O$ equation of Kim and O'Neil (1997). Using carbonate growth temperature of 35 ± 5 °C near sea level and 20 ± 10 °C in the Baca Formation area, we obtain a $\Delta\delta^{18}O_w$ of −8.3 ± 3.2 ‰. The model of Rowley (2007) for modern sites at low latitudes (<35°N) gives a paleoelevation estimate of 3880 m +778/−1064 m. Model uncertainties associated with unknown mean starting temperature and relative humidity of air masses is +675/−844 m (1σ) for this $\Delta\delta^{18}O_w$ value (Rowley, 2007).

Both approaches predict approximately modern to higher-than-modern paleoelevations during Baca deposition. Using a different distillation model adjusted for higher air temperature and relative humidity at low latitudes, as expected for the Eocene, would result in a lower isotopic lapse rate and thus in a higher paleoelevation estimate (Rowley, 2007; Hoke and others, 2014). However, Rowley's distillation model is designed for sites receiving a single moisture source (Rowley and others, 2001; Rowley and Garzione, 2007; Rowley, 2007) and neither approach takes into account the dual, monsoonal-related behavior observed in the modern $\delta^{18}O_c$-elevation relationship. Nor do they accommodate the possible influence of evaporation at low altitudes.

An alternate, and probably more realistic approach incorporates the probable impact of monsoons on the $\delta^{18}O_c$ value of Eocene soil carbonate. Climate simulations support the existence of strong North American monsoons during the Eocene (Sewall and others, 2000; Sewall an Sloan, 2006; Huber and Goldner, 2012; Feng and Poulsen, 2016), suggesting that significant summer monsoonal rainfall could have influenced the $\delta^{18}O_c$-elevation relationship at high altitude, mirroring trends observed in the modern data set. An intense hydrological cycle during the Eocene is likely to have increased the amount effect in summer precipitation (Licht and others, 2014), thereby diminishing the difference between winter and summer $\delta^{18}O_w$ (fig. 4B). However, Eocene winter and annual temperatures exceeding today's by 5 to 10 °C would have promoted the year-round growth of soil carbonate at higher altitudes, elevating the lapse rate transition by 700 to 1400 m, assuming that adiabatic lapse rates were similar-to-modern during the Eocene (fig. 3). Using slightly lower adiabatic lapse rates from climate simulations with Eocene boundary conditions (~5 °C per 1000 m gain; Feng and Poulsen, 2016) shifts the isotopic lapse rate transition to even higher elevations. This potential temperature effect would have favored evaporation over other controls on Eocene $\delta^{18}O_c$ values from samples obtained from sites ≤1900 to 3000 m of altitude, thereby raising the elevation of the reversal in $\delta^{18}O_c$ values. Accordingly, we argue that the Eocene $\delta^{18}O_c$-elevation relationship was primarily controlled by evaporation, resulting in a non-systematic decrease of $\delta^{18}O_c$ values with elevation increase, similar to that observed in modern data sets from low altitudes within the monsoonal domain and the Mojave Desert. Using the two similar lapse rates for soils below 1600 m (3.1 and 3.4 ‰/km), we obtain paleoelevation estimates for the Baca Formation of 1471 m ± 806 m and 1613 m ± 735 m (table 3). These estimates are roughly ~2 to 3 km lower than estimates from the two standard approaches; however, these estimates do not take into account potential change in regional aridity during the Eocene that could significantly modify the isotopic lapse rate in the evaporative domain (Quade and others, 2007a). Higher temperatures during the Eocene period are expected to result in increased evaporation. Stronger evaporation inland and at higher altitude would have increased the difference between the observed $\delta^{18}O_c$-elevation relationship, and that predicted from the $\delta^{18}O_w$ lapse rate of meteoric waters at higher elevations (fig. 4B). We thus suggest that our reconstructions likely underestimate paleoelevation and thus provide minimum estimates only.

Regardless of the chosen approach for determining the paleoelevation, all estimates suggest that significant elevation was already acquired in the southern part of the Colorado Plateau by the latter part of the Laramide orogeny (~38 Ma). Standard approaches using distillation modeling or modern precipitation lapse rate yield approximately modern to higher-than-modern paleoelevation estimates for the late Eocene, and thus ascribe all uplift of the Colorado Plateau to a Laramide deformation mechanism. Our approach is more conservative and suggests that the Baca Basin valley floor was located at paleoelevation above at least ~1 km during the Eocene. Given this estimate, our study suggests that at least half of the modern elevation of the southern Colorado Plateau was acquired by 38 Ma. This estimate favors syn-Laramide uplift mechanisms for the Colorado Plateau, such as those related to the set-up and early demise of the Farallon flat slab (Humphreys and others, 2003; Liu and Gurnis, 2010) or to intracrustal flow from the overthickened Sevier orogenic hinterland (Mc Quarrie and Chase, 2000) but does not preclude minor (<1km) post-Laramide uplift episodes to achieve the current elevation of the Baca basin and an implicitly complex Neogene uplift history for the Colorado Plateau (Flowers, 2010). The scattered character and the complexity of the $\delta^{18}O_c$-elevation relationship in the American Southwest precludes any precise paleoaltimetry estimate and does not allow us to draw more unequivocal conclusions.

CONCLUSION

This study has shown that: (1) the $\delta^{18}O_c$-elevation relationship in the American Southwest appears to be non-linear by reversing slope at 1200 to 1600 m of elevation; (2) Changes in evaporation intensity and carbonate growth season with altitude, combined with differences in the seasonality of rainfall are interpreted as the main causes of this scattering; (3) basic hypotheses on the evolution of this $\delta^{18}O_c$-elevation relationship and mid-Cenozoic $\delta^{18}O_c$ values permit us to suggest that at least half of the modern elevation of the southern Colorado Plateau was acquired by late in the history of Laramide deformation.

Our results highlight several important issues concerning the use of stable isotope paleo-altimetry in complex hydrological systems. First, our results reveal the non-systematic character of the $\delta^{18}O_c$-elevation relationship in the soils of regions receiving significant contributions from both summer and winter rainfall -despite the robust linear $\delta^{18}O_w$-elevation relationship observed for meteoric waters throughout the American Southwest (Blash and Bryson, 2007). These findings show the limitations of standard $\delta^{18}O_c$-elevation models based on isotopic $\delta^{18}O_w$ lapse rates or distillation models (for example, Rowley and others, 2001; Rowley and Garzione, 2007; Quade and others, 2007a), which can lead to significantly overestimate paleoelevations in this particular context. Variation in length of the carbonate growth season with elevation is not surprising and has been previously documented in the central Andes, where dominance of summer rainfall at low altitude delays carbonate growth until fall (Peters and others, 2013). Presence of two different moisture sources for rainfall has been shown to modify rainwater $\delta^{18}O_w$-elevation relationship on opposite sides of the same orogen (Quade and others, 2011; Hoke and others, 2013; Schemmel and others, 2013). To our knowledge ours is the first time that a non-linear lapse rate has been shown to influence $\delta^{18}O_c$-elevation relationship on a single altitudinal gradient. The lack of documentation of such a phenomenon is nonetheless unsurprising because most of the mountain ranges and plateaus where $\delta^{18}O$-elevation relationships have been characterized (for example, Sierra Nevada, Rockies, Andes, Anatolian Plateau, and the Himalayas) are high enough to block inland moisture penetration, and therefore receive precipitation derived from a single moisture source (Poage and Chamberlain, 2001; Quade and others, 2011; Hoke and others, 2009, 2013; Schemmel and others, 2013). Indeed, lower paleoelevations of these orogens might have (1) allowed greater penetration and mixing of moisture sources on both flanks, and (2) diminished the amount of orographic rainfall, potentially resulting in increased soil evaporation. While some workers have attempted to model the impact of these changes on the $\delta^{18}O_w$-elevation relationship (Ehlers and Poulsen, 2009; Poulsen and othersChen, 2010), our study highlights the challenges in interpreting the past relationship between $\delta^{18}O_c$ and elevation in such settings.

Although our paleoelevation estimates for the Baca Formation are qualitative only, they suggest that significant elevation was already acquired in the southern part of the Colorado Plateau by late Eocene time (Flowers and others, 2008). Uncertainties regarding the behavior of the $\delta^{18}O_c$-elevation relationship do not allow us to precisely quantify the paleoaltitude of the Eocene Baca Basin and thus determine the amount of potential post-Baca uplift.

ACKNOWLEDGMENTS

This work has been supported by the University of Arizona, the Comer Science and Education Foundation, and by Exxon-Mobil Corporation. A.L. was also funded by a Fyssen Foundation study grant. We thank D. Dettman and C. Eastoe for sharing their expertise on American Southwest hydrology and for access to the stable isotope facility, R. Lunt for thin section preparation, P. DeCelles, W. Dickinson, R. Spencer, R. Waldrip, J. Chapman, W. Skillings, R. Leary, B. Quade and M. Sabrié for prolific discussions and assistance in the field. We also thank Joe Galewsky and one anonymous reviewer for their constructive comments that greatly improved the manuscript.

APPENDIX

Table A1

Modern soils

Site	Sample	$\delta^{18}O$ V-PDB	STD	$\delta^{13}C$ V-PDB	STD
Baja California					
Site 1.	SB3_0.75_3	-3.97	0.048	-5.19	0.010
N28°58'13.0" W113°34'12.9"	SB3_0.75_4	-4.36	0.061	-5.20	0.033
Elevation 66 m	SB3_0.75_5	-5.90	0.040	-5.33	0.031
Bk depth: 65 cm	SB3_0.75_6	-4.32	0.014	-5.02	0.034
	SB3_0.75_7	-4.65	0.022	-3.82	0.047
	SB3_0.75_8	-5.56	0.083	-5.24	0.024
	SB3_0.75_1	-5.13	0.045	-3.85	0.027
	SB3_0.75_2	-6.33	0.017	-5.82	0.027
Site 2a.	SB2_0.6_1	-2.86	0.036	-6.67	0.039
N28°40'55.8" W114°04'21.5"	SB2_0.6_2	-3.85	0.042	-8.65	0.013
Elevation 125 m	SB2_0.6_3	-1.31	0.063	-6.49	0.012
Bk depth: 60 cm					
Site 2b.	SB1_1.0_1	-5.38	0.029	-3.43	0.025
N28°43'20.6" W114°05'45.8"	SB1_1.0_2	-5.75	0.019	-4.43	0.024
Elevation 142 m	SB1_1.0_3	-5.62	0.042	-3.51	0.042
Bk depth: 100 cm					
Site 3.	SB4_0.6_2	-3.92	0.075	-3.78	0.010
N28°59'06.6" W113°44'10.4"	SB4_0.6_1	-5.02	0.015	-3.20	0.015
Elevation 278 m	SB4_0.6_3	-5.59	0.032	-5.44	0.009
Bk depth: 60 cm	SB4_0.6_4	-5.57	0.036	-6.01	0.009
	SB4_0.6_05	-5.67	0.037	-5.67	0.037
	SB4_0.6_06	-5.87	0.047	-5.98	0.034
	SB4_0.6_07	-5.64	0.059	-5.62	0.018
	SB4_0.6_08	-5.68	0.043	-5.58	0.012
Site 4.	SB5_1.0_1	-1.19	0.062	-3.15	0.033
N29°39'12.2" W114°38'14.2"	SB5_1.0_2	-1.87	0.061	-4.17	0.022
Elevation 670 m	SB5_1.0_3	-2.63	0.057	-3.66	0.051
Bk depth: 100 cm	SB5_1.0_4	-1.68	0.032	-2.83	0.024
	SB5_1.0_3	-2.67	0.012	-4.06	0.005
Arizona / New Mexico					
Site 5. Tumamoc Hill	TUM 80-90 A1	-3.11	0.050	-3.89	0.024
N32°13'18.7" W111°00'39.0"	TUM 80-90 A2	-2.70	0.115	-3.59	0.035
Elevation 710 m	TUM 80-90 A3	-3.83	0.053	-3.55	0.037
Bk depth: 85 (samples TUM	TUM 80-90 A4	-3.44	0.042	-3.89	0.052
80-90), 95 (samples TUM 90-	TUM 80-90 B	-3.39	0.088	-3.33	0.046
100), 79 to 89 (samples	TUM 80-90 C	-3.20	0.032	-3.91	0.007
AZPIMA1), 95 to 140	TUM 80-90 D	-3.90	0.014	-3.85	0.028
(samples AZPIMA 3) and 70	TUM 90-100 A	-4.31	0.059	-4.46	0.026
to 130 (samples AZPIMA2)	TUM 90-100 C	-4.45	0.013	-3.59	0.042
cm	TUM 90-100 D	-4.11	0.050	-4.29	0.029
	AZPIMA1 79	-3.06	0.052	-1.89	0.033
	AZPIMA1 80	-3.41	0.024	-2.72	0.020

Table A1
(continued)

Site	Sample	δ[18]O V-PDB	STD	δ[13]C V-PDB	STD
Arizona / New Mexico					
Site 5. Tumamoc Hill	AZPIMA1 84 A1	-3.86	0.019	-2.42	0.035
N32°13'18.7" W111°00'39.0"	AZPIMA1 84 A2	-3.61	0.051	-2.46	0.025
Elevation 710 m	AZPIMA1 89	-4.33	0.078	-2.98	0.028
Bk depth: 85 (samples TUM	AZPIMA3 95-100A	-4.38	0.067	-2.09	0.024
80-90), 95 (samples TUM 90-	AZPIMA3 95-100B	-4.60	0.044	-2.17	0.040
100), 79 to 89 (samples	AZPIMA3 115-20	-5.77	0.055	-2.14	0.032
AZPIMA1), 95 to 140	AZPIMA3 140	-4.72	0.038	-2.03	0.022
(samples AZPIMA 3) and 70	AZPIMA2 70-80 A1	-3.77	0.086	-2.76	0.089
to 130 (samples AZPIMA2)	AZPIMA2 70-80 B1	-2.73	0.105	-1.20	0.060
cm	AZPIMA2 70-80 B2	-4.16	0.096	-1.96	0.017
	AZPIMA2 100-110	-3.83	0.092	-2.63	0.039
	AZPIMA2 125-130	-3.74	0.057	-3.48	0.029
Site 6. Hougton Road	HOU_0.6_03	-8.05	0.081	-5.59	0.020
N32°04'10.8" W110°46'23.1"	HOU_0.6_01	-8.38	0.072	-3.81	0.027
Elevation 914 m	HOU_0.6_02	-8.10	0.026	-3.97	0.014
Bk depth: 60 cm	HOU_0.6_04	-7.79	0.231	-4.50	0.040
	HOU_0.6_05	-7.04	0.039	-1.82	0.042
	HOU_0.6_06	-6.93	0.079	-0.78	0.040
	HOU_0.6_07	-7.52	0.034	-3.45	0.046
	HOU_0.6_08	-6.17	0.076	-5.42	0.026
Site 7. Pantano Road	PTN_0.7_02	-5.32	0.028	-1.77	0.045
N32°00'23.7" W110°35'21.2"	PTN_0.7_03	-6.22	0.047	-1.30	0.042
Elevation 1075 m	PTN_0.7_04	-7.65	0.027	-1.92	0.009
Bk depth: 70 cm	PTN_0.7_05	-6.41	0.025	-2.88	0.028
	PTN_0.7_06	-5.30	0.006	-1.82	0.031
	PTN_0.7_08	-7.11	0.051	-1.82	0.019
	PTN_0.7_07	-5.95	0.072	-2.07	0.021
Site 8. Pinalenos Mnts	PM2(1.2M)-1	-9.87	0.024	-8.82	0.037
N32°41'05.5" W109°45'32.3"	PM2(1.2M)-2	-9.44	0.019	-8.44	0.025
Elevation 1229 m	PM2(1.2M)-3	-9.80	0.086	-8.58	0.061
Bk depth: 120 cm	PM2(1.2M)-4	-9.01	0.127	-4.63	0.014
	PM2(1.2M)-5	-8.85	0.031	-4.47	0.032
	PM2(1.2M)_06	-9.14	0.012	-8.40	0.017
	PM2(1.2M)_07	-9.06	0.078	-8.49	0.029
	PM2(1.2M)_08	-9.33	0.055	-8.18	0.020
	PM2(1.2M)_09	-10.06	0.009	-8.55	0.029
Site 9. Hirabayashi Arroyo	HIR 57	-8.74	0.150	-7.78	0.059
N31°07'09.4" W110°02'16.1"	HIR 67 B1	-9.23	0.080	-7.75	0.037
Elevation 1451 m	HIR 72 A1 (r1)	-9.24	0.142	-7.80	0.052
Bk depth: 57 (sample HIR	HIR 72 B2	-9.35	0.077	-7.25	0.048
57), 67 (sample HIR 67), 72	HIR 72 D1 (r1)	-8.82	0.109	-7.71	0.046
(samples HIR72) cm					

Table A1

(continued)

Site	Sample	$\delta^{18}O$ V-PDB	STD	$\delta^{13}C$ V-PDB	STD
Arizona / New Mexico					
Site 10. French Joe Canyon	FJC 60-5 A1	-7.89	0.033	-6.69	0.026
N31°48'32.6" W110°23'24.9"	FJC 60-5 A2	-7.06	0.027	-5.50	0.038
Elevation 1523 m	FJC 60-5 B	-8.72	0.063	-5.46	0.017
Bk depth: 60 to 100 (samples	FJC 60-5 C	-8.79	0.049	-5.10	0.012
FJC), 160 to 180 (samples	FJC 60-5 D	-7.11	0.117	-5.32	0.030
FJC A) cm	FJC 60-5 E	-8.90	0.110	-0.30	0.032
	FJC 60-5 F	-10.60	0.038	-5.55	0.021
	FJC 60-5 G	-8.76	0.019	-5.09	0.025
	FJC C 70-80 B1	-9.13	0.081	-6.38	0.032
	FJC C 70-80 B2	-9.90	0.042	-8.51	0.046
	FJC C 70-80 B3	-9.84	0.020	-8.41	0.014
	FJC C 70-80 B4	-9.62	0.009	-7.98	0.027
	FJC 80-90	-8.40	0.041	-3.04	0.021
	FJC 80-90	-9.32	0.130	-4.48	0.085
	FJC 90-100 A	-5.32	0.087	-2.23	0.016
	FJC 90-100 B	-8.73	0.034	-1.41	0.024
	FJC 90-100 C	-8.66	0.021	-5.41	0.022
	FJC A 160	-8.41	0.064	-5.95	0.035
	FJC A 170-190 B1	-10.11	0.082	-5.49	0.063
Site 11. Huachuca Mntns N	HUACNA55-B1(P)	-9.11	0.055	1.23	0.017
N32°00'24.4" W110°43'02.6"	HUACNA55-B2	-7.48	0.043	-0.87	0.011
Elevation 1823 m	HUACNA63-H1OUT	-6.22	0.033	-0.88	0.033
Bk depth: 55 to 70 cm	HUACNA63-A5OUT	-5.29	0.035	-2.10	0.040
	HUACNA 63 A6-P	-7.90	0.029	-2.77	0.021
	HUACNA 63 B3 P	-8.44	0.050	-2.15	0.061
	HUACNA 67 A3 P	-8.03	0.051	-1.55	0.032
	HUACNA67 A4(P)	-8.24	0.032	-2.34	0.014
	HUACNA 65-75 A1	-8.29	0.092	-2.18	0.024
	HUACNA 65-75 B1	-7.44	0.039	-1.35	0.039
	HUACNA 65-75 B2	-7.72	0.140	-2.60	0.063
	HUACNA 65-75 C2	-7.95	0.115	-1.99	0.081
	HUACNA 50-60 A1	-7.49	0.046	-1.17	0.022
	HUACNA 60-5 A1	-7.97	0.088	-2.77	0.039
	HUACNA 60-5 A2	-8.10	0.027	-2.35	0.015
	HUACNA 60-5 A3	-8.30	0.057	-2.75	0.032
	HUACNA 60-5 A4	-7.96	0.037	-2.04	0.038
	HUACNA 60-5 B1	-8.54	0.062	-2.32	0.026
Site 12. Huachuca Mntns S	HUACSA 60 B2	-7.49	0.088	-4.02	0.019
N31°07'09.4" W110°02'16.1"	HUACSA 60 A2	-5.56	0.045	-4.66	0.033
Elevation 1910 m	HUACSA 60 A3	-8.14	0.033	-0.55	0.015
Bk depth: 55 to 85 (samples	HUACSA 60 A4	-7.34	0.037	-4.21	0.013
HUACSA and HUACSB), 80	HUACSA 85 B2	-7.51	0.013	-4.44	0.028
to 120 (samples HUACSC)	HUACSA 85 B3	-7.24	0.038	-4.82	0.030
cm	HUACSA 63 G1	-8.03	0.033	-4.86	0.016
	HUACSA 63 G2	-8.19	0.059	-4.53	0.020
	HUACSA 63 H1	-7.89	0.034	-4.04	0.041
	HUACSA 63 I1	-8.24	0.053	-4.83	0.038
	HUACSA 63 J1	-8.04	0.016	-4.85	0.010
	HUACSA 63 K1	-7.94	0.059	-4.93	0.015
	HUACSA 63 L1	-8.28	0.066	-4.78	0.041
	HUACSA 63 M1	-8.48	0.041	-4.01	0.030

Table A1
(continued)

Site	Sample	$\delta^{18}O$ V-PDB	STD	$\delta^{13}C$ V-PDB	STD
Arizona / New Mexico					
Site 12. Huachuca Mntns S	HUACSA 55 A1	-5.84	0.011	-4.04	0.027
N31°07'09.4" W110°02'16.1"	HUACSA 55 A2	-7.38	0.040	-4.30	0.035
Elevation 1910 m	HUACSA 55 A3	-7.60	0.025	-3.95	0.023
Bk depth: 55 to 85 (samples	HUACSA 55 B1	-7.62	0.046	-4.53	0.038
HUACSA and HUACSB), 80	HUACSA 55 B2	-5.47	0.033	-4.68	0.031
to 120 (samples HUACSC)	HUACSA 65 A1	-5.84	0.082	-4.18	0.019
cm	HUACSA 65 A2	-5.44	0.044	-4.78	0.048
	HUACSA 65 A3	-5.54	0.091	-4.52	0.034
	HUACSA 65 A5	-7.16	0.090	-3.99	0.016
	HUACSB 65 A	-7.86	0.061	-2.76	0.027
	HUACSB 65 B	-7.75	0.067	-3.66	0.024
	HUACSB 65 C	-8.28	0.038	-4.86	0.016
	HUACSB 65 D	-8.21	0.057	-4.07	0.024
	HUACSB 65 E	-8.13	0.060	-4.83	0.010
	HUACSC 115 C1	-7.88	0.013	-4.09	0.020
	HUACSC 115 D1	-8.11	0.045	-4.50	0.015
	HUACSC 115 C2	-8.02	0.028	-4.17	0.020
	HUACSC 80-90 A1	-7.78	0.080	-4.64	0.025
	HUACSC 80-90 B1	-6.72	0.039	-3.93	0.037
	HUACSC 110-20 A1	-7.99	0.025	-4.35	0.025
	HUACSC 110-20 B1	-8.18	0.073	-4.39	0.027
Site 13. Baca River	SM18(90CM)-1	-6.00	0.012	-5.63	0.033
N34°21'16.8" W107°59'25.2"	SM18(90CM)-2	-7.94	0.114	-5.73	0.080
Elevation 2348 m	SM18(90CM)-3	-5.72	0.072	-5.58	0.025
Bk depth: 90 cm	SM18(90CM)-4	-5.79	0.026	-5.56	0.010
	SM18(90CM)-5	-6.14	0.047	-5.49	0.035
	SM18(90CM)-6	-5.68	0.038	-5.57	0.021
	SM18(90CM)-7	-6.26	0.050	-5.86	0.024
	SM18(90CM)-8	-6.09	0.047	-5.60	0.016
Site 14. Sawtooth Mntns	SM17_0.7_1	-6.53	0.017	-2.78	0.045
N34°19'34.1" W107°59'18.4"	SM17_0.7_2	-6.41	0.076	-3.10	0.038
Elevation 2425 m	SM17_0.7_3	-6.23	0.022	-2.40	0.018
Bk depth: 70 (samples	SM17_0.7_4	-6.25	0.032	-2.13	0.049
SM17_0.7), 100 (samples	SM17_1.0_5	-6.25	0.068	-2.35	0.018
SM17_1.0) cm	SM17_1.0_6	-5.87	0.025	-2.60	0.032
	SM17_1.0_1	-6.14	0.024	-2.20	0.074
	SM17_1.0_2	-6.40	0.029	-2.49	0.021
	SM17_1.0_7	-7.03	0.003	-3.07	0.021
	SM17_1.0_8	-7.23	0.043	-2.57	0.025
	SM17_1.0_3	-9.14	0.041	-6.36	0.019

Table A2

Eocene carbonates

Site	Sample	Description	$\delta^{18}O$ V-PDB	STD	$\delta^{13}C$ V-PDB	STD
REJECTED SITES						
Mineta Formation (Oligocene, San Pedro Trough, Arizona) Mineta Ridge Section N32°17'53.6" W110°28'05.9"	MR-24	Lacustrine Limestone. 37 m	-19.72	0.017	1.32	0.019
	MR-25-A	Lacustrine Limestone. 39 m	-19.80	0.016	3.95	0.012
	MR-16	Lacustrine Limestone. 48 m	-19.30	0.010	3.51	0.016
	MR-17-A	Lacustrine Limestone. 56 m	-17.19	0.124	3.27	0.045
	MR-18-A	Lacustrine Limestone. 63 m	-20.92	0.029	3.48	0.031
	MR-19	Lacustrine Limestone. 74.5 m	-18.98	0.040	4.23	0.003
	MR-20-A	Lacustrine Limestone. 82 m	-22.27	0.056	3.41	0.037
	MR-13-A	Lacustrine Limestone. 91 m	-20.48	0.061	5.37	0.063
	MR-21-A	Lacustrine Limestone. 99 m	-20.59	0.025	3.19	0.054
	MR-22	Lacustrine Limestone. 104.5 m	-18.31	0.030	4.01	0.039
	MR-14-A	Lacustrine Limestone. 110 m	-13.15	0.020	3.63	0.031
	MR-15-A	Marl. 115 m	-18.19	0.011	1.94	0.032
	MR-26-A	Lacustrine limestone (Cement). 128 m	-21.57	0.035	1.31	0.047
	MR-26-B	Lacustrine limestone (clast). 128 m	-19.53	0.056	1.60	0.013
	MR-27	Lacustrine Limestone. 131 m	-12.72	0.072	4.17	0.036
	MR-29	Lacustrine Limestone. 143 m	-17.55	0.031	-0.57	0.015
	MR-30	Lacustrine Limestone. 144.5 m	-17.63	0.013	-1.32	0.031
	MR-31	Lacustrine Limestone. 148 m	-21.71	0.007	-0.48	0.020
	MR-28-A	Lacustrine Limestone. 148.5 m	-15.97	0.016	-0.34	0.007
	MR-32	Marl. 153 m	-14.72	0.024	-1.59	0.016
	MR-33	Marl. 159 m	-17.28	0.006	-1.12	0.042
	MR-34-A	Marl. 165 m	-15.33	0.029	-2.65	0.021
	MR-35-A	Marl. 171 m	-15.76	0.061	-2.39	0.032
	MR-38	Marl. 173.5 m	-16.39	0.015	-4.22	0.019
	MR-36	Marl. 178.5 m	-16.30	0.048	-1.75	0.024
	MR-39	Marl. 180.5 m	-15.51	0.010	-3.95	0.007
	MR-37	Marl. 186 m	-14.12	0.039	-2.54	0.005
	MR-40	Marl. 192 m	-21.01	0.089	-1.68	0.030
	MR-41	Marl. 198.5 m	-12.48	0.006	-4.82	0.027
	MR-42	Marl. 206 m	-14.21	0.099	-2.48	0.010
	MR-43	Marl. 219 m	-12.86	0.017	-3.82	0.019
	MR-44	Marl. 222 m	-10.76	0.033	-1.34	0.031
	MR-45	Marl. 230 m	-15.61	0.030	-3.57	0.041
	MR-46	Lacustrine Limestone. 242 m	-15.27	0.029	-1.36	0.012
	MR-47	Lacustrine Limestone. 245.5 m	-15.73	0.049	-1.92	0.016
	MR-07	Lacustrine Limestone. 250 m	-11.01	0.008	-0.97	0.035
	MR-09-A	Lacustrine Limestone. 255.5 m	-11.33	0.011	1.35	0.007
	MR-48	Lacustrine Limestone. 265 m	-10.13	0.039	-0.79	0.021
	MR-10	Lacustrine Limestone. 271.5 m	-9.04	0.064	-4.13	0.054
	MR-11	Lacustrine Limestone. 276 m	-6.00	0.047	0.49	0.026
	MR-12	Lacustrine Limestone. 281 m	-7.40	0.024	2.58	0.017
American Flag Formation (Late Cretaceous, Catalina Mountains, Arizona) N32°32'04.1" W110°43'03.9"	AF-01	Conglomerate (carbonate clast)	-12.88	0.007	-4.38	0.008
	AF-02	Conglomerate (matrix)	-15.25	0.025	-1.40	0.030
	AF-03	Conglomerate (matrix)	-14.16	0.019	-3.72	0.003
	AF-04	Conglomerate (matrix)	-10.77	0.070	-3.52	0.009
	AF-05	Conglomerate (carbonate clast)	-17.96	0.026	-5.05	0.033
Lobo Formation (Paleocene – Early Eocene, New Mexico) Florida Mountains section N32°08'22.7" W107°38'56.0"	FM1-2	Pedogenic nodule. 2 m	-18.09	0.095	-5.96	0.054
	FM1-8.1	Pedogenic nodule. 8.1 m	-17.64	0.066	-5.24	0.032
	FM1-11.3	Pedogenic nodule. 11.3 m	-17.06	0.062	-5.61	0.058
	FM1-18.5	Pedogenic nodule. 18.5 m	-15.66	0.021	-4.98	0.005
	FM1-19.8	Pedogenic nodule. 19.8 m	-15.23	0.020	-5.10	0.027
	FM1-21.5	Lacustrine Limestone. 21.5 m	-13.68	0.010	-5.44	0.018
	FM1-27.5	Lacustrine Limestone. 27.5 m	-13.54	0.008	-5.58	0.035
	FM1-29.8	Sandstone (cement). 29.8 m	-13.45	0.049	-3.05	0.025
	FM1-77	Sandstone (cement). 77 m	-12.82	0.022	-3.61	0.029
	FM1-96.5	Sandstone (cement). 96.5 m	-12.14	0.043	-3.55	0.033

TABLE A2

(continued)

Site	Sample	Description	$\delta^{18}O$ V-PDB	STD	$\delta^{13}C$ V-PDB	STD
REJECTED SITES						
Lobo Formation (Paleocene – Early Eocene, New Mexico) Florida Mountains section N32°08'22.7" W107°38'56.0"	FM1-107	Sandstone (cement). 107 m	-12.15	0.057	-2.84	0.025
	FM1-119	Sandstone (cement). 119 m	-12.41	0.081	-3.31	0.021
	FM1-127	Sandstone (cement). 127 m	-12.39	0.033	-2.92	0.020
	FM1-140	Sandstone (cement). 140 m	-12.33	0.021	-3.05	0.018
	FM1-151.5	Sandstone (cement). 151.5 m	-12.36	0.010	-3.85	0.031
	FM1-161	Sandstone (cement). 161 m	-14.84	0.036	-4.87	0.038
	FM1-166	Sandstone (cement). 166 m	-12.97	0.025	-4.02	0.037
	FM1-178.5	Sandstone (cement). 178.5 m	-13.71	0.072	-2.92	0.044
	FM1-189	Sandstone (cement). 189 m	-14.82	0.033	-2.42	0.004
Lobo Formation Vittorio Mountains section N32°11'50.1" W108°06'43.3"	VM-1	Carbonate nodule	-17.09	0.051	-4.82	0.022
	VM-2	Carbonate nodule	-16.80	0.051	-5.44	0.024
	VM-3	Carbonate nodule	-17.35	0.014	-5.27	0.027
	VM-4	Carbonate nodule	-17.58	0.028	-6.26	0.006
Fort Crittenden Formation (Late Cretaceous, Arizona) Santa Rita Mountains Gardner & Adobe Canyons N31°41'13.7" W110°45'56.8"	GC01	Sandstone (cement).	-17.94	0.020	-8.44	0.025
	GC02-A	Pedogenic Nodule.	-18.11	0.019	-8.86	0.012
	GC4	Pedogenic Nodule.	-13.59	0.023	-7.93	0.014
	GC5	Pedogenic Nodule.	-14.84	0.011	-7.30	0.013
	AC1-A	Freswater bivalve.	-13.33	0.051	-4.93	0.035
	AC1-B	Freswater bivalve.	-16.12	0.002	-5.02	0.048
	AC1-C	Freswater bivalve.	-13.71	0.072	-0.94	0.014
	AC2-A	Freswater bivalve.	-12.59	0.036	-1.84	0.050
Mission Valley Formation (Late Eocene, California) Old Quarry Section N32°47'12.7" W117°07'43.6"	MS09_A_0.6_1	Pedogenic Nodule.	-12.02	0.012	-6.97	0.045
	MS09_A_0.6_2	Pedogenic Nodule.	-11.39	0.008	-7.00	0.025
	MS09_B_0.6_1	Pedogenic Nodule.	-12.16	0.058	-6.19	0.007
	MS09_B_0.6_2	Pedogenic Nodule.	-12.38	0.005	-6.20	0.008
	MS09_C_1.1_1	Pedogenic Nodule.	-11.93	0.009	-6.38	0.024
	MS09_C_1.1_2	Pedogenic Nodule.	-12.10	0.067	-6.70	0.024
	MS09_D2_0.6	Pedogenic Nodule.	-11.43	0.065	-7.13	0.029
	MS09_D1_0.6	Pedogenic Nodule.	-12.07	0.019	-6.39	0.035
Frias Formation (Late Eocene, California) Stone crest road Section N32°48'20.4" W117°07'03.6"	MS10_A_0.4_1	Pedogenic Nodule.	-10.74	0.053	-5.93	0.031
	MS10_A_0.4_2	Pedogenic Nodule.	-10.68	0.014	-5.91	0.011
	MS10_A_0.8_1	Pedogenic Nodule.	-10.48	0.041	-6.42	0.038
	MS10_A_0.8_2	Pedogenic Nodule.	-10.40	0.055	-6.22	0.015
	MS10_B_0.8_1	Pedogenic Nodule.	-10.23	0.083	-7.92	0.017
	MS10_B_0.8_2	Pedogenic Nodule.	-10.00	0.051	-7.76	0.041
Amole Arkose (Late Cretaceous, Arizona) Tucson Mountains N32°14'16" W111°08'37"	AA_1	Lacustrine Limestone.	-14.62	0.209	-5.26	0.060
	AA_2	Lacustrine Limestone.	-15.84	0.018	-7.20	0.027
	AA_3	Lacustrine Limestone.	-12.38	0.033	-7.78	0.018
	AA_4	Lacustrine Limestone.	-12.80	0.018	-4.24	0.011
Pantano Formation (Oligocene, Arizona) N31°59'25.1" W110°38'08.9"	PF01	Sandstone (cement)	-7.32	0.027	-6.96	0.017
	PF02	Sandstone (cement)	-10.49	0.066	-1.16	0.058
	PF03	Sandstone (cement)	-10.44	0.023	-1.65	0.027
	PF04	Marl	-6.93	0.029	-6.13	0.032
	PF05	Sandstone (cement)	-10.68	0.049	-2.23	0.039
	PF06	Sandstone (cement)	-12.82	0.038	-2.35	0.010
	PF07	Sandstone (cement)	-8.35	0.196	-5.28	0.054
	PF10	Sandstone (cement)	-7.88	0.114	-4.27	0.042
	PF11	Sandstone (cement)	-11.06	0.008	-0.29	0.004
	PF12	Sandy limestone	-10.47	0.059	-1.68	0.025
	PF13	Sandstone (cement)	-9.94	0.035	-2.52	0.014

TABLE A2

(continued)

Site	Sample	Description	$\delta^{18}O$ V-PDB	STD	$\delta^{13}C$ V-PDB	STD
REJECTED SITES						
Pantano Formation (Oligocene, Arizona) N31°59'25.1" W110°38'08.9"	PF14	Sandstone (cement)	-9.76	0.047	-0.57	0.032
	PF15	Lacustrine Limestone.	-10.20	0.068	-2.73	0.024
	PF16	Lacustrine Limestone.	-9.98	0.013	-0.39	0.038
	PF17	Lacustrine Limestone.	-12.19	0.029	-0.64	0.060
	PF18	Lacustrine Limestone.	-11.65	0.044	4.52	0.033
	PF19-1	Lacustrine Limestone.	-11.30	0.017	1.17	0.034
	PF19-2A	Lacustrine Limestone.	-11.54	0.053	0.66	0.020
	PF19-2B	Lacustrine Limestone.	-10.36	0.059	1.12	0.049
Mineta Formation (Oligocene, San Pedro Trough, Arizona) Teran Wash Section N32°16'13.6" W110°17'19.2"	TW03	Lacustrine Limestone. 14.5 m	-8.25	0.044	3.68	0.057
	TW04	Lacustrine Limestone. 21 m	-7.88	0.051	4.51	0.028
	TW05	Lacustrine Limestone. 34 m	-9.32	0.056	6.50	0.009
	TW06	Lacustrine Limestone. 40.5 m	-14.34	0.058	2.71	0.022
	TW07	Lacustrine Limestone. 48.5 m	-8.55	0.002	5.51	0.006
	TW08	Lacustrine Limestone. 57 m	-7.88	0.024	5.46	0.003
	TW09	Lacustrine Limestone. 65 m	-7.97	0.021	4.72	0.014
	TW10	Lacustrine Limestone. 75 m	-9.12	0.008	7.07	0.048
	TW11	Lacustrine Limestone. 87.5 m	-8.79	0.057	7.24	0.038
	TW13	Marl. 103 m	-7.78	0.070	1.92	0.013
	TW12	Marl. 120 m	-8.90	0.080	-2.48	0.011
	TW14	Marl. 131.5 m	-8.29	0.016	-2.88	0.022
	TW15	Lacustrine Limestone. 148 m	-5.63	0.065	5.93	0.018
	TW17	Carbonate lens in gypsum bed. 159.5 m	-4.19	0.065	0.55	0.012
	TW19	Carbonate lens in gypsum bed. 179 m	-5.91	0.029	1.62	0.003
	TW20	Carbonate lens in gypsum bed. 191 m	-7.82	0.014	-0.28	0.007
	TW21	Carbonate lens in gypsum bed. 198 m	-6.89	0.029	4.02	0.009
	TW23	Carbonate lens in gypsum bed. 225 m	-5.25	0.013	3.27	0.130
	TW37	Carbonate lens in gypsum bed. 226 m	-5.25	0.048	2.47	0.011
	TW24	Lacustrine Limestone. 231 m	-6.66	0.020	2.81	0.046
	TW25	Lacustrine Limestone. 246.5 m	-6.70	0.039	2.91	0.010
	TW26	Lacustrine Limestone. 259 m	-5.09	0.011	4.10	0.051
	TW27	Lacustrine Limestone. 267 m	-3.85	0.023	3.99	0.021
	TW28	Lacustrine Limestone. 278.5 m	-4.20	0.033	4.39	0.056
	TW30	Lacustrine Limestone. 294 m	-5.13	0.024	3.14	0.025
	TW31	Lacustrine Limestone. 308.5 m	-5.90	0.029	2.22	0.024
	TW32	Lacustrine Limestone. 318.5 m	-7.38	0.031	2.85	0.027
	TW33	Lacustrine Limestone. 332 m	-5.22	0.078	2.94	0.011
	TW34	Lacustrine Limestone. 345 m	-6.40	0.029	2.70	0.013
	TW35	Lacustrine Limestone. 356 m	-6.88	0.009	2.98	0.029
	TW38	Lacustrine Limestone. 352 m	-6.98	0.028	2.74	0.036
	TW36	Lacustrine Limestone. 366 m	-7.09	0.042	3.67	0.029
	TW39	Lacustrine Limestone. 363 m	-8.76	0.043	1.07	0.020
	TW40	Lacustrine Limestone. 378 m	-11.20	0.062	1.96	0.037
SELECTED SITES						
Baca Formation (Late Eocene, New Mexico) Mariana Mesa area N34°21'47.0" W108°29'26.4"	BFS-1	Pedogenic nodule – stage 1 calcrete	-9.09	0.064	-5.54	0.040
	BFS-1.5-01	Pedogenic nodule – stage 1 calcrete	-12.39	0.155	-4.02	0.028
	BFS-1.5-02	Pedogenic nodule – stage 1 calcrete	-10.67	0.014	-4.80	0.036
	BFS-1.5-03	Pedogenic nodule – stage 1 calcrete	-10.33	0.061	-5.08	0.016
	BFS-2	Pedogenic nodule – stage 1 calcrete	-9.21	0.012	-6.73	0.022
	BFS-3	Pedogenic nodule – stage 1 calcrete	-9.04	0.076	-5.19	0.036
	BFS-4	Pedogenic nodule – stage 1 calcrete	-10.32	0.006	-5.18	0.034
	BFS-5-01	Pedogenic nodule – stage 1 calcrete	-10.58	0.022	-6.81	0.031
	BFS-5-02	Pedogenic nodule – stage 1 calcrete	-10.59	0.018	-6.66	0.020
	BFS-5-03	Pedogenic nodule – stage 1 calcrete	-10.59	0.020	-6.45	0.013
	BFS-5-04	Pedogenic nodule – stage 1 calcrete	-10.61	0.108	-6.61	0.007
	BFS-6-01	Pedogenic nodule – stage 2 calcrete	-9.29	0.009	-6.36	0.031
	BFS-6-02	Pedogenic nodule – stage 2 calcrete	-10.37	0.053	-6.06	0.005
	BFS-6-03	Pedogenic nodule – stage 2 calcrete	-10.37	0.019	-6.16	0.012
	BFS-6-04	Pedogenic nodule – stage 2 calcrete	-10.35	0.050	-6.10	0.021

Table A2
(continued)

Site	Sample	Description	$\delta^{18}O$ V-PDB	STD	$\delta^{13}C$ V-PDB	STD
SELECTED SITES						
Baca Formation	SM05	Pedogenic nodule – stage 1 calcrete	-8.49	0.056	-6.70	0.120
(Late Eocene, New Mexico)	SM07	Pedogenic nodule – stage 1 calcrete	-10.43	0.072	-7.71	0.012
Sawtooth Mntns	SM8-00	Pedogenic nodule – stage 2 calcrete	-10.73	0.022	-6.99	0.010
N34°19'42.3"	SM8-01	Pedogenic nodule – stage 2 calcrete	-9.82	0.045	-7.17	0.040
W108°00'09.8"	SM8-02	Pedogenic nodule – stage 2 calcrete	-9.88	0.022	-7.14	0.014
	SM8-03	Pedogenic nodule – stage 2 calcrete	-9.79	0.022	-7.18	0.010
	SM11	Pedogenic nodule – stage 1 calcrete	-10.39	0.046	-9.33	0.015
	SM12	Pedogenic nodule – stage 1 calcrete	-9.79	0.075	-6.07	0.044
	SM13	Pedogenic nodule – stage 1 calcrete	-9.13	0.059	-4.19	0.037
Lomas Las Tetas de Cabra	TC2(2.5M)_1	Pedogenic nodule – stage 2 calcrete	-0.27	0.049	-6.41	0.004
Formation (Early Eocene,	TC2(2.5M)_2	Pedogenic nodule – stage 2 calcrete	-0.89	0.022	-6.49	0.019
Baja California)	TC2(2.5M) 03	Pedogenic nodule – stage 2 calcrete	-2.48	0.027	-6.56	0.015
N28°41'02.9"	TC2(2.5M) 04	Pedogenic nodule – stage 2 calcrete	-2.90	0.025	-6.66	0.011
W114°04'57.7"	TC2(2.5M) 05	Pedogenic nodule – stage 2 calcrete	-2.43	0.006	-6.59	0.029
	TC3_0.6_1	Pedogenic nodule – stage 3 calcrete	-6.00	0.075	-6.80	0.025
	TC3_0.6_2	Pedogenic nodule – stage 3 calcrete	-6.07	0.024	-6.99	0.022
	TC3_0.6_03	Pedogenic nodule – stage 3 calcrete	-7.16	0.081	-6.75	0.011
	TC3_0.6_04	Pedogenic nodule – stage 3 calcrete	-6.96	0.005	-6.72	0.013
	TC3_0.6_05	Pedogenic nodule – stage 3 calcrete	-7.11	0.007	-6.73	0.010
	TC3_0.6_06	Pedogenic nodule – stage 3 calcrete	-7.14	0.021	-6.78	0.045
	TC4(1M) 01	Pedogenic nodule – stage 1 calcrete	-6.41	0.003	-8.50	0.021
	TC4(1M) 02	Pedogenic nodule – stage 1 calcrete	-6.14	0.026	-8.29	0.000
	TC4(1M) 03	Pedogenic nodule – stage 1 calcrete	-6.27	0.031	-8.41	0.020
	TC4(1M) 04	Pedogenic nodule – stage 1 calcrete	-6.30	0.067	-8.32	0.042
	TC4(1M) 05	Pedogenic nodule – stage 1 calcrete	-6.28	0.031	-8.54	0.014

TABLE A3

Clumped isotopes

	Sample	Analysis ID	$\delta^{13}C$ V-PDB	$\delta^{13}C$ std	$\delta^{18}O$ V-PDB	$\delta^{18}O$ std	Δ47 ARF	Δ47 std	Δ48	$\delta^{13}C$ carb mean	$\delta^{13}C$ carb SE	$\delta^{18}O$ carb mean	$\delta^{18}O$ carb SE	Δ47 ARF mean	Δ47 std	Expected from standards 0.024	T (°C) from Kelson and others	T SE (°C)
Mineta Formation – Teran Wash	TW04	140730_9_TW04	4.159	0.074	-8.749	0.132	0.544	0.013	0.707	4.03	0.05	-8.68	0.07	0.519	0.015	0.008	58	6
		140801_7_TW04	4.062	0.005	-8.627	0.007	0.480	0.008	0.536									
		140808_8_TW04	3.925	0.004	-8.826	0.006	0.541	0.008	0.691									
		140806_10_TW04	3.973	0.005	-8.521	0.008	0.510	0.008	0.778									
	TW06	140728_3_TW06	2.819	0.005	-14.226	0.007	0.519	0.008	0.944	2.80	0.01	-14.15	0.04	0.524	0.036	0.014	56	14
		140731_8_TW06	2.809	0.005	-14.091	0.007	0.465	0.010	0.821									
		140908_1_TW06	2.768	0.008	-14.120	0.015	0.588	0.009	1.966									
	TW11	140730_5_TW11	6.237	0.044	-9.501	0.077	0.513	0.014	0.388	6.32	0.06	-9.27	0.10	0.497	0.011	0.012	68	6
		140805_6_TW11	6.314	0.004	-9.069	0.007	0.515	0.008	0.963									
		140806_8_TW11	6.219	0.004	-9.164	0.007	0.468	0.008	0.796									
		140908_2_TW11	6.498	0.005	-9.361	0.008	0.493	0.009	0.555									
	TW27	140728_5_TW27	3.985	0.004	-5.966	0.007	0.564	0.010	0.446	3.89	0.06	-5.59	0.26	0.551	0.019	0.012	45	7
		140801_5_TW27	3.787	0.005	-5.860	0.008	0.526	0.009	0.533									
		140807_2_TW27	3.799	0.005	-5.686	0.008	0.514	0.008	0.612									
		140908_4_TW27	4.001	0.005	-4.835	0.008	0.598	0.009	0.506									
	TW33	140731_7_TW33	3.049	0.005	-5.070	0.008	0.522	0.008	0.641	2.94	0.07	-5.14	0.14	0.540	0.007	0.012	49	5
		140807_8_TW33	3.066	0.004	-4.845	0.008	0.538	0.010	0.469									
		140808_7_TW33	2.775	0.004	-5.128	0.007	0.552	0.008	0.554									
		140907_6_TW33	2.867	0.005	-5.513	0.007	0.549	0.009	0.934									
Pantano Formation	PF15	140730_1_PF15	3.431	0.096	-12.922	0.173	0.532	0.017	1.163	3.17	0.20	-12.75	0.07	0.526	0.020	0.012	55	8
		140805_7_PF15	3.348	0.005	-12.616	0.008	0.485	0.009	0.747									
		140914_4_PF15	2.581	0.005	-12.775	0.010	0.578	0.010	0.983									
		140807_1_PF15	3.306	0.004	-12.688	0.008	0.508	0.008	1.399									
	PF16	140730_6_PF16	-0.458	0.096	-12.697	0.174	0.517	0.016	0.753	-0.59	0.08	-12.60	0.10	0.535	0.032	0.014	51	13
		140805_9_PF16	-0.564	0.004	-12.376	0.006	0.491	0.008	0.563									
		140914_5_PF16	-0.758	0.005	-12.728	0.009	0.598	0.008	0.452									
	PF17	140729_10_PF17	0.256	0.045	-11.444	0.083	0.436	0.013	0.524	0.24	0.05	-11.30	0.07	0.431	0.023	0.012	105	14
		140801_3_PF17	0.250	0.004	-11.299	0.007	0.402	0.009	0.430									
		140806_6_PF17	0.107	0.004	-11.118	0.008	0.391	0.008	0.955									
		140914_2_PF17	0.351	0.006	-11.355	0.013	0.494	0.012	0.299									

Table A3

(continued)

	Sample	Analysis ID	δ13C V-PDB	δ13C std	δ18O V-PDB	δ18O std	Δ47 ARF	Δ47 std	Δ48	δ13C carb mean	δ13C carb SE	δ18O carb mean	δ18O carb SE	Δ47 ARF mean	Δ47 std	Expected from standards 0.024	T (°C) from Kelson and others	T SE (°C)
Pantano Formation	PF18	140914_3_PF18	0.463	0.005	-10.656	0.009	0.531	0.010	0.529	0.07	0.23	-11.00	0.46	0.495	0.014	0.012	69	7
		140806_9_PF18	-0.576	0.004	-12.366	0.008	0.470	0.008	0.601									
		140807_9_PF18	0.329	0.004	-10.525	0.006	0.504	0.007	0.488									
		140731_5_PF18	0.055	0.004	-10.469	0.007	0.475	0.009	0.311									
	PF19-1	140728_2_PF19-1	0.966	0.010	-11.358	0.018	0.616	0.008	0.661	1.04	0.05	-11.32	0.07	0.607	0.018	0.012	25	6
		140914_1_PF19_1	1.188	0.004	-11.494	0.008	0.653	0.010	0.885									
		140731_3_PF19-1	0.969	0.005	-11.229	0.007	0.585	0.008	0.319									
		140808_2_PF19-1	1.055	0.005	-11.211	0.008	0.573	0.009	0.690									
Baca Formation - Sawtooth Mountains	SM05	140730_10_SM05	-6.583	0.089	-9.242	0.165	0.608	0.015	0.266	-6.68	0.05	-9.12	0.09	0.575	0.012	0.012	36	4
		140801_2_SM05	-6.612	0.004	-9.282	0.007	0.549	0.010	0.354									
		140808_5_SM05	-6.769	0.004	-9.069	0.007	0.568	0.009	0.274									
		140805_2_SM05	-6.748	0.004	-8.885	0.008	0.573	0.008	1.889									
	SM07	140805_4_SM07	-7.955	0.004	-10.788	0.007	0.598	0.010	0.156	-7.80	0.10	-10.87	0.04	0.574	0.008	0.012	36	4
		140730_8_SM07	-7.702	0.048	-10.985	0.090	0.573	0.011	-0.225									
		140801_6_SM07	-7.569	0.004	-10.848	0.008	0.564	0.009	0.429									
		140808_4_SM07	-7.983	0.004	-10.840	0.007	0.561	0.008	0.410									
	SM08	140729_3_SM08	-6.661	0.006	-11.207	0.009	0.620	0.009	0.768	-6.87	0.09	-10.84	0.20	0.608	0.024	0.012	25	7
		140801_1_SM08	-6.817	0.004	-11.008	0.009	0.664	0.008	1.666									
		140806_1_SM08	-6.890	0.004	-10.864	0.006	0.548	0.009	0.458									
		140808_10_SM08	-7.106	0.004	-10.297	0.009	0.602	0.009	0.372									
	SM11	140806_2_SM11	-4.541	0.004	-14.340	0.008	0.529	0.007	0.476	-4.38	0.06	-14.67	0.27	0.519	0.010	0.012	58	5
		140806_5_SM11	-4.395	0.004	-14.139	0.009	0.542	0.011	1.830									
		140808_3_SM11	-4.364	0.004	-14.842	0.008	0.498	0.007	0.471									
		140908_5_SM11	-4.226	0.005	-15.349	0.007	0.506	0.008	0.953									
	SM12	140808_9_SM12	-3.369	0.005	-15.984	0.009	0.523	0.010	0.677	-4.32	0.32	-12.79	1.07	0.567	0.022	0.012	39	8
		140801_4_SM12	-4.583	0.004	-11.933	0.008	0.541	0.008	0.343									
		140806_3_SM12	-4.720	0.004	-11.521	0.009	0.586	0.010	0.896									
		140730_4_SM12	-4.598	0.079	-11.736	0.145	0.619	0.018	0.856									
Mineta Fm (Mineta Ridge)	MR25	140728_4_MR25	3.734	0.005	-20.280	0.008	0.378	0.008	1.030									
	MR21	140728_6_MR21	3.180	0.005	-20.875	0.010	0.448	0.007	0.867									
	MR09	140730_3_MR09	1.102	0.013	-12.012	0.024	0.409	0.009	0.916									

Table A3

(continued)

	Sample	Analysis ID	$\delta^{13}C$ V-PDB	$\delta^{13}C$ std	$\delta^{18}O$ V-PDB	$\delta^{18}O$ std	Δ47 ARF	Δ47 std	Δ48	$\delta^{13}C$ carb mean	$\delta^{13}C$ carb SE	$\delta^{18}O$ carb mean	$\delta^{18}O$ carb SE	Δ47 ARF mean	Δ47 std	Expected from standards 0.024	T (°C) from Kelson and others	T SE (°C)
Lobo Fm	FM1-21.5	140729_4_FM1-21.5	-5.151	0.005	-14.091	0.008	0.373	0.008	0.515									
(Florida	FM1-11.3	140729_9_FM1-11.3	-5.554	0.027	-17.717	0.046	0.381	0.012	1.197									
Mountains)	FM1-19.8	140731_4_FM-19.8	-5.042	0.005	-15.565	0.009	0.328	0.008	0.375									
		Analysis screened for contamination (D48 >2 per mil)																
	TW06	140807_5_TW06	2.584	0.005	-13.782	0.011	0.398	0.008	5.660									

Clumped isotope analysis ($\delta^{18}O$, $\delta^{13}C$ and Δ47) of carbonate samples was performed at the University of Washington. Carbonate samples and standards (5–9 mg) were digested for 10 minutes at 90 °C in a common bath of phosphoric acid (specific gravity 1.90–1.95). The evolved CO_2 was cryogenically separated from water and purified on an automated stainless steel vacuum line, which used He as the carrier gas to pass the CO2 through a Porapaq Q trap (50/80 mesh, 15 cm long, 4.5 mm ID, 0.635 mm OD) held between −15 °C and −17 °C for a transfer time of 15 minutes. Carbonate standards were prepared, for every four samples, using the same procedure. Purified CO_2 was transferred to Pyrex break seals and loaded into an automated 10-port tube cracker inlet system on a Thermo MAT 253 mass spectrometer configured to measure masses 44–49 inclusive. Δ47 values were calculated using established methods (Brand and others, 2010; Schauer and others, 2016) and were corrected to the absolute reference frame (ARF) of Dennis and others (2011) using analyses of CO_2 that had been equilibrated with two waters that differed in Δ47 by ~ 40 ‰ at 4 and 60 °C as well as CO_2 that had been heated to 1000°C. Sample Δ48 values were used to screen for contamination (Δ48 > 2 ‰ rejected). Carbonate temperature (T(Δ47)) was calculated from measured Δ47 values using the calibration of Kelson and others (2017).

REFERENCES

Adams, D. K., and Comrie, A. C., 1997, The North American Monsoon: Bulletin of the American Meteorological Society, v. 78, p. 2197–2213, https://doi.org/10.1175/1520-0477(1997)078<2197:TNAM>2.0.CO;2

Amato, J. M., 2000, Structural relationships in the Florida Mountains, southwestern New Mexico - A review, *in* Lawton, T. F., McMillan, N. J., and McLemore, V. T., editors, Southwest Passage-A trip through the Phanerozoic: New Mexico Geologic Society Guidebook, 51st Field Conference, p. 103–108.

Bayona, G., and Lawton, T. F., 2003, Fault-Proximal stratigraphic record of episodic extension and oblique inversion, Bisbee basin, southwestern New Mexico, USA: Basin Research, v. 15, n. 2, p. 251–270, https://doi.org/10.1046/j.1365-2117.2003.00199.x

Blash, K. W., and Bryson, J. R., 2007, Distinguishing Sources of Ground Water Recharge by Using δ^2H and δ^{18}O: Ground Water, v. 45, n. 3, p. 294–308, https://doi.org/10.1111/j.1745-6584.2006.00289.x

Bird, P., 1979, Continental delamination and the Colorado Plateau: Journal of Geophysical Research-Solid Earth, v. 84, n. B13, p. 7561–7571, https://doi.org/10.1029/JB084iB13p07561

Boggs, S., Jr., 2009, Petrology of Sedimentary Rocks: Cambridge, England, Cambridge University Press, 600 p.

Brand, W. A., Assonov, S. S., and Coplen, T. B., 2010, Correction for the ^{17}O interference in $\delta(^{13}$C) measurements when analyzing CO_2 with stable isotope mass spectrometry (IUPAC Technical Report): Pure and Applied Chemistry, v. 82, n. 8, p. 1719–1733, http://dx.doi.org/10.1351/PAC-REP-09-01-05

Breecker, D. O., Sharp, Z. D., and McFadden, L. D., 2009, Seasonal bias in the formation and stable isotopic composition of pedogenic carbonate in modern soils from central New Mexico, USA: G.S.A. Bulletin, v. 121, n. 3–4, p. 630–640, https://doi.org/10.1130/B26413.1

Bristow, T. F., Bonifacie, M., Derkowski, A., Eiler, J. M., and Grotzinger, J. P., 2011, A hydrothermal origin for isotopically anomalous cap dolostone cements from south China: Nature, v. 474, p. 68–71, https://doi.org/10.1038/nature10096

Buck, B. J., and Mack, G. H., 1995, Latest Cretaceous (Maastrichtian) aridity indicated by paleosols in the McRae Formation, south-central New Mexico: Cretaceous Research, v. 16, n. 5, p. 559–572, https://doi.org/10.1006/cres.1995.1036

Cassel, E. J., Graham, S. A., and Chamberlain, C. P., 2009, Cenozoic tectonic and topographic evolution of the northern Sierra Nevada, California, through stable isotope paleoaltimetry in volcanic glass: Geology, v. 37, n. 6, p. 547–550, https://doi.org/10.1130/G25572A.1

Cather, S., and Johnson, B., 1984, Eocene tectonics and depositional setting of west-central New Mexico and eastern Arizona New Mexico: Bureau of Mines and Mineral Resources Circular, n. 192, p. 1–33.

Cather, S. M., Connell, S. D., Chamberlin, R. M., McIntosh, W. C., Jones, G. E., Potochink, A. R., Lucas, S. G., and Johnson, P. S., 2008, The Chuska erg: Paleogeomorphic and paleoclimatic implications of an Oligocene sand sea on the Colorado Plateau: GSA Bulletin, v. 120, n. 1–2, p. 13–33, https://doi.org/10.1130/B26081.1

Cather, S. M., Chapin, C. E., and Kelley, S. A., 2012, Diachronous episodes of Cenozoic erosion in southwestern North America and their relationship to surface uplift, paleoclimate, paleodrainage, and paleoaltimetry: Geosphere, v. 8, n. 6, p. 1177–1206, https://doi.org/10.1130/GES00801.1

Chamberlain, C. P., Mix, H. T., Mulch, A., Hren, M. T., Kent-Corson, M. L., Davis, S. J., Horton, T. W., and Graham, S. A., 2012, The Cenozoic climatic and topographic evolution of the western North American Cordillera: American Journal of Science, v. 312, n. 2, p. 213–262, https://doi.org/10.2475/02.2012.05

Clay, D., ms, 1970, Stratigraphy and petrology of the Mineta Formation in Pima and eastern Cochise Counties, Arizona: Tucson, Arizona, University of Arizona, Tucson, Ph. D. thesis, 221 p., http://hdl.handle.net/10150/565218

Clinkscales, C., and Lawton, T., 2015, Timing of Late Cretaceous shortening and basin development, Little Hatchet Mountains, southwestern New Mexico, USA – implications for regional Laramide tectonics: Basin Research, v. 27, n. 4, p. 453–472, https://doi.org/10.1111/bre.12083

Copeland, P., Murphy, M. A., Dupré, W. R., and Lapen, T. J., 2011, Oligocene Laramide deformation in southern New Mexico and its implications for Farallon plate geodynamics: Geosphere, v. 7, n. 5, p. 1209–1219, https://doi.org/10.1130/GES00672.1

Dennis, K., Affek, H., Passey, B., Schrag, D., and Eiler, J., 2011, Defining an absolute reference frame for 'clumped' isotope studies of CO_2: Geochimica et Cosmochimica Acta, v. 75, n. 22, p. 7117–7131, https://doi.org/10.1016/j.gca.2011.09.025

Dettman, D. L., and Lohmann, K. C., 2000, Oxygen isotope evidence for high-altitude snow in the Laramide Rocky Mountains of North America during the Late Cretaceous and Paleogene: Geology, v. 28, n. 3, p. 243–246, https://doi.org/10.1130/0091-7613(2000)28<243:OIEFHS>2.0.CO;2

Deutz, P., Montanez, I. P., and Curtis Monger, H. C., 2002, Morphology and stable and radiogenic isotope composition of pedogenic carbonates in late Quaternary relict soils, New Mexico, U.S.A.: An integrated record of pedogenic overprinting: Journal of Sedimentary Research, v. 72, n. 6, p. 809–822, https://doi.org/10.1306/040102720809

Dickinson, W. R., 1991, Tectonic setting of faulted Tertiary strata associated with the Catalina core complex in southern Arizona: GSA Special Paper, v. 264, p. 1–106, https://doi.org/10.1130/spe264-p1

Ding, L., Xu, Q., Yue, Y., Wang, H., Cai, F., and Li, S., 2014, The Andean-type Gangdese Mountains: Paleoelevation record from the Paleocene–Eocene Linzhou Basin: Earth and Planetary Science Letters, v. 392, p. 250–264, https://doi.org/10.1016/j.epsl.2014.01.045

Douglas, M. W., Maddox, R. A., Howard, K., and Reyes, S., 1993, The Mexican Monsoon: Journal of Climate, v. 6, p. 1665–1677, https://doi.org/10.1175/1520-0442(1993)006<1665:TMM>2.0.CO;2

Dutton, A., Wilkinson, B. H., Welker, J. M., Bowen, G. J., and Lohmann, K. C., 2005, Spatial distribution and

seasonal variation in $^{18}O/^{16}O$ of modern precipitation and river water across the conterminous USA: Hydrological Processes, v. 19, n. 20, p. 4121–4146, https://doi.org/10.1002/hyp.5876
Eastoe, C. J., and Dettman, D. L., 2016, Isotope amount effects in hydrologic and climate reconstructions of monsoon climates: Implications of some long-term data sets for precipitation: Chemical Geology, v. 430, p. 78–89, https://doi.org/10.1016/j.chemgeo.2016.03.022
Elhers, T. A., and Poulsen, C. J., 2009, Influence of Andean uplift on climate and paleoaltimetry estimates: Earth and Planetary Science Letters, v. 281, n. 3–4, p. 238–248, https://doi.org/10.1016/j.epsl.2009.02.026
Environmental Isotope Laboratory (EIL), 2015, Stable O + H isotopes in Tucson precipitation 1981-2012 monthly averages, dataset submitted to IAEA: Available online at http://www.geo.arizona.edu/node/154. University of Arizona.
Fan, M., and Dettman, D. L., 2009, Late Paleocene high Laramide ranges in northeast Wyoming: Oxygen isotope study of ancient river water: Earth and Planetary Science Letters, v. 286, n. 1–2, p. 110–121, https://doi.org/10.1016/j.epsl.2009.06.024
Fan, M., Hough, B. G., and Passey, B. H., 2014, Middle to late Cenozoic cooling and high topography in the central Rocky Mountains: Constraints from clumped isotope geochemistry: Earth and Planetary Science Letters, v. 408, p. 35–47, https://doi.org/10.1016/j.epsl.2014.09.050
Feng, T., and Poulsen, C. J., 2016, Refinement of Eocene lapse rates, fossil-leaf altimetry, and North American Cordilleran surface elevation estimates: Earth and Planetary Science Letters, v. 436, p. 130–141, https://doi.org/10.1016/j.epsl.2015.12.022
Flowers, R. M., 2010, The enigmatic rise of the Colorado Plateau: Geology, v. 38, n. 7, p. 671–672, https://doi.org/10.1130/focus072010.1
Flowers, R. M., and Farley, K. A., 2012, Apatite $^{4}He/^{3}He$ and (U-Th)/He evidence for an ancient Grand Canyon: Science, v. 338, n. 6114, p. 1616–1619, https://doi.org/10.1126/science.1229390
Flowers, R. M., Wernicke, B. P., and Farley, K. A., 2008, Unroofing, incision, and uplift history of the southwestern Colorado Plateau from apatite (U-Th)/He thermochronometry: GSA Bulletin, v. 120, n. 5–6, p. 571–587, https://doi.org/10.1130/B26231.1
Flynn, J. J., Cipolletti, R. M., and Novacek, M. J., 1989, Chronology of early Eocene marine and terrestrial strata, Baja California, Mexico: GSA Bulletin, v. 101, n, 9, p. 1182–1196, https://doi.org/10.1130/0016-7606(1989)101<1182:COEEMA>2.3.CO;2
Fricke, H. C., 2003, Investigation of early Eocene water-vapor transport and paleoelevation using oxygen isotope data from geographically widespread mammal remains: Geological Society of America Bulletin, v. 115, n. 9, p. 1088–1096, https://doi.org/10.1130/B25249.1
Fricke, H. C., and Wing, S. L., 2004, Oxygen isotope and paleobotanical estimates of temperature and $\delta^{18}O$-latitude gradients over North America during the early Eocene: American Journal of Science, v. 204, n. 7, p. 612–635, https://doi.org/10.2475/ajs.304.7.612
Fricke, H., Foreman, B. Z., and Sewall, J. O., 2010, Integrated climate model-oxygen isotope evidence for a North American monsoon during the Late Cretaceous: Earth and Planetary Science Letters, v. 289, n. 1–2, p. 11–21, https://doi.org/10.1016/j.epsl.2009.10.018
Galewsky, J., 2009, Orographic precipitation isotopic ratios in stratified atmospheric flows: Implications for paleoelevation studies: Geology, v. 37, n. 9, p. 791–794, https://doi.org/10.1130/G30008A.1
Gallagher, T. M., and Sheldon, N. D., 2016, Combining soil water balance and clumped isotopes to understand the nature and timing of pedogenic carbonate formation: Chemical Geology, v. 435, p. 79–91, https://doi.org/10.1016/j.chemgeo.2016.04.023
Gile, L. H., Peterson, F. F., and Grossman, R. B., 1966, Morphological and genetic sequences of carbonate accumulation in desert soils: Soil Science, v. 101, n. 5, p. 347–360, https://doi.org/10.1097/00010694-196605000-00001
González-León, C. M., and Lawton, T. F., 1995, Stratigraphy, depositional environments, and origin of the Cabullona basin, northeastern Sonora, *in* Jacques-Ayala, C., González-León, C. M., and Roldán-Quintana, J., editors, Studies on the Mesozoic of Sonora and adjacent areas: Geological Society of America Special Paper, v. 301, p. 121–142, https://doi.org/10.1130/0-8137-2301-9.121
Greenwood, D. R., and Wing, S. L., 1995, Eocene continental climates and latitudinal temperature gradients: Geology, v. 23, n. 11, p. 1044–1048, https://doi.org/10.1130/0091-7613(1995)023<1044:ECCALT>2.3.CO;2
Grimm, J., ms, 1978, Cenozoic pisolitic limestones of Pima and Cochise Counties, Arizona: Tucson, Arizona, University of Arizona, Master thesis, 81 p.
Grover, J. A., 1984, Petrology, depositional environments and structural development of the Mineta Formation, Teran Basin, Cochise County, Arizona: Sedimentary Geology, v. 38, n. 1–4, p. 87–105, https://doi.org/10.1016/0037-0738(84)90075-7
Henkes, G. A., Passey, B. H., Grossman, E. L., Shenton, B. J., Perez-Huerta, A., and Yancey, T. E., 2015, Temperature limits for preservation of primary calcite clumped isotope paleotemperatures: Geochimica et Cosmochimica Acta, v. 139, p. 362–382, https://doi.org/10.1016/j.gca.2014.04.040
Hoke, G. D., Garzione, C. N., Araneo, D. C., Latorre, C., Strecker, M. R., and Williams, K. J., 2009, The stable isotope altimeter: Do Quaternary pedogenic carbonates predict modern elevations?: Geology, v. 37, n. 11, p. 1015–1018, https://doi.org/10.1130/G30308A.1
Hoke, G. D., Aranibar, J. N., Viale, M., Araneo, D. C., and Llano, C., 2013, Seasonal moisture sources and the isotopic composition of precipitation, rivers, and carbonates across the Andes at 32.5–35.5°S: Geochemistry, Geophysics, Geosystems, v. 14, n. 4, p. 962–978, https://doi.org/10.1002/ggge.20045
Hoke, G. D., Zeng, J., Hren, M. T., Wissinka, G. K., and Garzione, C. N., 2014, Stable isotopes reveal high southeast Tibetan Plateau margin since the Paleogene: Earth and Planetary Science Letters, v. 394, p. 270–278, https://doi.org/10.1016/j.epsl.2014.03.007
Hough, B. G., Fan, M., and Passey, B. H., 2014, Calibration of the clumped isotope geothermometer in soil

carbonate in Wyoming and Nebraska, USA: Implications for paleoelevation and paleoclimate reconstruction: Earth and Planetary Science Letters, v. 391, p. 110–120, https://doi.org/10.1016/j.epsl.2014.01.008
Hren, M. T., Pagani, M., Erwin, D. M., and Brandon, M., 2010, Biomarker reconstruction of the early Eocene paleotopography and paleoclimate of the northern Sierra Nevada: Geology, v. 38, n. 1, p. 7–10, https://doi.org/10.1130/G30215.1
Huber, M., and Goldner, A., 2012, Eocene Monsoons: Journal of Asian Earth Sciences, v. 44, p. 3–23, https://doi.org/10.1016/j.jseaes.2011.09.014
Humphreys, E., Hessler, E., Dueker, K., Farmer, G. L., Erslev, E., and Atwater, T., 2003, How Laramide-age hydration of North American lithosphere by the Farallon slab controlled subsequent activity in the western United States: International Geology Review, v. 45, n. 7, p. 575–595, https://doi.org/10.2747/0020-6814.45.7.575
Huntington, K. W., and Lechler, A. R., 2015, Carbonate clumped isotope thermometry in continental tectonics: Tectonophysics, v. 647–648, p. 1–20, https://doi.org/10.1016/j.tecto.2015.02.019
Huntington, K. W., Wernicke, B. P., and Eiler, J. M., 2010, Influence of climate change and uplift on Colorado Plateau paleotemperatures from carbonate clumped isotope thermometry: Tectonics, v. 29, n. 3, TC3005, https://doi.org/10.1029/2009TC002449
Huntington, K. W., Budd, D. A., Wernicke, B. P., and Eiler, J. M., 2011, Use of Clumped-isotope thermometry to constrain the crystallization temperature of diagenetic calcite: Journal of Sedimentary Research, v. 81, n. 9, p. 656–669, https://doi.org/10.2110/jsr.2011.51
Huntington, K. W., Saylor, J., Quade, J., and Hudson, A. M., 2015, High late Miocene–Pliocene elevation of the Zhada Basin, southwestern Tibetan Plateau, from carbonate clumped isotope thermometry: Geological Society of America Bulletin, v. 127, n. 1–2, p. 181–199, https://doi.org/10.1130/B31000.1
Inman, K., 1987, Depositional environments and sandstone petrography of Cretaceous sedimentary rocks, Adobe Canyon, Santa Rita Mountains, southeastern Arizona, *in* Dickinson, W., and Klute, M., editors, Mesozoic rocks of southern Arizona and adjacent areas: Arizona Geological Society Digest, v. 18, p. 301–314.
James, C. N., and Houze, R. A., 2005, Modification of precipitation by coastal orography in storms crossing northern California: Monthly Weather Review, v. 133, n. 11, p. 3110–3131, https://doi.org/10.1175/MWR3019.1
Karlstrom, K. E., Lee, J. P., Kelley, S. A., Crow, R. S., Crossey, L. J., Young, R. A., Lazear, G., Beard, L. S., Richetts, J. W., Fox, M., and Shuster, D. L., 2014, Formation of the Grand Canyon 5 to 6 million years ago through integration of older palaeocanyons: Nature Geoscience, v. 7, p. 239–244, https://doi.org/10.1038/ngeo2065
Kelson, J. R., Huntington, K. W., Schauer, A. J., Saenger, C., and Lechler, A. R., 2017, Toward a universal carbonate clumped isotope calibration: Diverse synthesis and preparatory methods suggest a single temperature relationship: Geochimica et Cosmochimica Acta, v. 197, p. 104–131, https://doi.org/10.1016/j.gca.2016.10.010
Kent-Corson, M. L., Sherman, L. S., Mulch, A., and Chamberlain, C. P., 2006, Cenozoic topographic and climatic response to changing tectonic boundary conditions in Western North America: Earth and Planetary Science Letters, v. 252, n. 3–4, p. 453–466, https://doi.org/10.1016/j.epsl.2006.09.049
Kent-Corson, M. L., Barnosky, A. D., Mulch, A., Carrasco, M. A., and Chamberlain, C. P., 2013, Possible regional tectonic controls on mammalian evolution in western North America: Palaeogeography, Palaeoclimatology, Palaeoecology, v. 387, p. 17–26, https://doi.org/10.1016/j.palaeo.2013.07.014
Kim, S., and O'Neil, J. R., 1997, Equilibrium and nonequilibrium oxygen isotope effects in synthetic carbonates: Geochimica et Cosmochimica Acta, v. 61, n. 16, p. 3461–3475, https://doi.org/10.1016/S0016-7037(97)00169-5
Knauth, L. P., and Kennedy, M. J., 2009, The Late Precambrian greening of the Earth: Nature, v. 460, p. 728–732, https://doi.org/10.1038/nature08213
Kowler, A. L., ms, 2007, The stable carbon and oxygen isotopic composition of pedogenic carbonate and its relationship to climate and ecology in southeastern Arizona: Tucson, Arizona, University of Arizona, M.S. thesis, 56 p.
Lawton, T. F., Basabilvazo, G. T., Hodgson, S. A., Wilson, D. A., Mack, G. H., McIntosh, W. C., Lucas, S. G., and Kietxke, K. K., 1993, Laramide stratigraphy of the Little Hatchet Mountains, southwestern New Mexico: New Mexico Geology, v. 15, p. 9–15.
Lechler, A. R., Niemi, N. A., Hren, M. T., and Lohman, K. C., 2013, Paleoelevation estimates for the northern and central proto–Basin and Range from carbonate clumped isotope thermometry: Tectonics, v. 32, n. 3, p. 295–316, https://doi.org/10.1002/tect.20016
Levander, A., Schmandt, B., Miller, M. S., Liu, K., Karlstrom, K. E., Crow, R. S., Lee, C.-T. A., and Humphreys, E. D., 2011, Continuing Colorado plateau uplift by delamination-style convective lithospheric downwelling: Nature, v. 472, p. 461–465, https://doi.org/10.1038/nature10001
Licht, A., van Cappelle, M., Abels, H. A., Ladant, J., Trabucho-Alexandre, J., France-Lanord, C., Donnadieu, Y., Vandenberghe, J., Rigaudier, T., Lecuyer, C., Terry Jr., D., Adriaens, R., Boura, A., Guo, Z., Aung Naing Soe, Dupont-Nivet, G., and Jaeger, J.-J., 2014, Asian monsoons in a late Eocene greenhouse world: Nature, v. 513, p. 501–506, https://doi.org/10.1038/nature13704
Liu, B., Phillips, F., Hoines, S., Campbell, A. R., and Sharma, P., 1995, Water movement in desert soil traced by hydrogen and oxygen isotopes, chloride, and chlorine-36, southern Arizona: Journal of Hydrology, v. 168, n. 1–4, p. 91–110, https://doi.org/10.1016/0022-1694(94)02646-S
Liu, B., Phillips, F. M., and Campbell, A. R., 1996, Stable carbon and oxygen isotopes of pedogenic carbonates, Ajo Mountains, southern Arizona: Implications for paleoenvironmental change: Palaeogeography, Palaeoclimatology, Palaeoecology, v. 124, n. 3–4, p. 233–246, https://doi.org/10.1016/0031-0182(95)00093-3

Liu, L., and Gurnis, M., 2010, Dynamic subsidence and uplift of the Colorado Plateau: Geology, v. 38, n. 7, p. 663–666, https://doi.org/10.1130/G30624.1
Lucas, S., 1983, The Baca formation and the Eocene-Oligocene Boundary in New Mexico, *in* Chapin, C. E., and Callender, J. F., editors, Socorro Region II: New Mexico Geological Society Guidebook, v. 2, p. 187–192.
Lucas, S. G., Lewis, C., Dickinson, W. R., and Heckert, A. B., 2005, The late Cretaceous Tucson Mountains dinosaur: New Mexico Museum of Natural History and Science Bulletin, v. 29, p. 105–110.
McQuarrie, N., and Chase, C. G., 2000, Raising the Colorado plateau: Geology, v. 28, p. 91–94, https://doi.org/10.1130/0091-7613(2000)028<0091:RTCP>2.0.CO;2
McQuarrie, N., and Wernicke, B. P., 2005, An animated tectonic reconstruction of southwestern North America since 36 Ma: Geosphere, v. 1, n. 3, p. 147–172, https://doi.org/10.1130/GES00016.1
Mix, H. T., Mulch, A., Kent-Corson, M. L., and Chamberlain, C. P., 2011, Cenozoic migration of topography in the North American Cordillera: Geology, v. 39, n. 1, p. 87–90, https://doi.org/10.1130/G31450.1
Moucha, R., Forte, A. M., Rowley, D. B., Mitrovica, J. X., Simmons, N. A., and Grand, S. P., 2009, Deep mantle forces and the uplift of the Colorado Plateau: Geophysical Research Letters, v. 36, n. 19, https://doi.org/10.1029/2009GL039778
Mulch, A., 2016, Stable isotope paleoaltimetry and the evolution of landscapes and life: Earth and Planetary Science Letters, v. 433, p. 180–191, https://doi.org/10.1016/j.epsl.2015.10.034
Mulch, A., Graham, S. A., and Chamberlain, C. P., 2006, Hydrogen isotopes in Eocene river gravels and paleoelevation of the Sierra Nevada: Science, v. 313, n. 5783, p. 87–89, https://doi.org/10.1126/science.1125986
Mulch, A., Teyssier, C., Cosca, M. A., and Chamberlain, C. P., 2007, Stable isotope paleoaltimetry of Eocene core complexes in the North American Cordillera: Tectonics, v. 26, n. 4, https://doi.org/10.1029/2006TC001995
Novacek, M. J., Ferrusquia-Villafranca, I., Flynn, J. J., Wyss, A. R., and Norell, M. A., 1991, Wasatchian (early Eocene) mammals and other vertebrates from Baja California, Mexico: The Lomas las Tetas de Cabra Fauna: Bulletin of the American Museum of Natural History, v. 208, p. 1–88, http://hdl.handle.net/2246/903
O'Brien, G. R., Kaufman, D. S., Sharp, W. D., Atudorei, V., Parnell, R. A., and Crossey, L. J., 2006, Oxygen isotope composition of annually banded modern and mid-Holocene travertine and evidence of paleomonsoon floods, Grand Canyon, Arizona, USA: Quaternary Research, v. 65, n. 3, p. 366–379, https://doi.org/10.1016/j.yqres.2005.12.001
Pagani, M., Zachos, J. C., Freeman, K. H., Tipple, B., and Bohaty, S., 2005, Marked decline in Atmospheric Carbon Dioxide Concentrations during the Paleogene: Science, v. 309, n. 5735, p. 600–603, https://doi.org/10.1126/science.1110063
Parsons, T., and McCarthy, J., 1995, The active southwest margin of the Colorado Plateau: Uplift of mantle origin: GSA Bulletin, v. 107, n. 2, p. 139–147, https://doi.org/10.1130/0016-7606(1995)107<0139:TASMOT>2.3.CO;2
Passey, B. H., and Henkes, G. A., 2012, Carbonate clumped isotope bond reordering and geospeedometry: Earth and Planetary Science Letters, v. 351–352, p. 223–236, https://doi.org/10.1016/j.epsl.2012.07.021
Peirce, H. W., Damon, P. E., and Shafiqullah, M., 1979, An Oligocene (?) Colorado plateau edge in Arizona: Tectonophysics, v. 61, n. 1–3, p. 1–24, https://doi.org/10.1016/0040-1951(79)90289-0
Peters, N. A., Huntington, K. W., and Hoke, G. D., 2013, Hot or not? Impact of seasonally variable soil carbonate formation on paleotemperature and O-isotope records from clumped isotope thermometry: Earth and Planetary Science Letters, v. 361, p. 208–218, https://doi.org/10.1016/j.epsl.2012.10.024
Poage, M. A., and Chamberlain, C. P., 2001, Empirical relationships between elevation and the stable isotope composition of precipitation and surface waters: Considerations for studies of paleoelevation change: American Journal of Science, v. 301, n. 1, p. 1–15, https://doi.org/10.2475/ajs.301.1.1
Poore, R. Z., Pavich, M. J., and Grissino-Mayer, H. D., 2005, Record of the North American southwest monsoon from Gulf of Mexico sediment cores: Geology, v. 33, n. 3, p. 209–212, https://doi.org/10.1130/G21040.1
Poulsen, C. J., Elhers, T. A., and Insel, N., 2010, Onset of Convective Rainfall During Gradual Late Miocene Rise of the Central Andes: Science, v. 328, n. 5977, p. 490–493, https://doi.org/10.1126/science.1185078
Prothero, D. R., Ludtke, J. A., and Lucas, S. G., 2004, Magnetic stratigraphy of the middle Eocene (Duchesnean) Baca Formation, West-Central New Mexico, *in* Lucas, S. G., Zeigler, K. E., and Kondrashov, P. E., editors, Paleogene Mammals: New Mexico Museum of Natural History and Science Bulletin, v. 26, p. 55–58.
Quade, J., Cerling, T. E., and Bowman, J. R., 1989, Systematic variations in the carbon and oxygen isotopic composition of pedogenic carbonate along elevation transects in the southern Great Basin, United States: GSA Bulletin, v. 101, n. 4, p. 464–475, https://doi.org/10.1130/0016-7606(1989)101<0464:SVITCA>2.3.CO;2
Quade, J., Garzione, C., and Eiler, J., 2007a, Paleoelevation reconstruction using pedogenic carbonates: Reviews in Mineralogy and Geochemistry, v. 66, n. 1, p. 53–87, https://doi.org/10.2138/rmg.2007.66.3
Quade, J., Rech, J. A., Latorre, C., Betancourt, J. L., Gleason, E., and Kalin, M. T. K., 2007b, Soils at the hyperarid margin: The isotopic composition of soil carbonate from the Atacama Desert: Geochimica et Cosmochima Acta, v. 71, n. 15, p. 3772–3795, https://doi.org/10.1016/j.gca.2007.02.016
Quade, J., Breecker, D. O., Daeron, M., and Eiler, J., 2011, The paleoaltimetry of Tibet: An isotopic perspective: American Journal of Science, v. 311, n. 2, p. 77–115, https://doi.org/10.2475/02.2011.01
Quade, J., Eiler, J., Daeron, M., and Achyuthan, H., 2013, The clumped isotope geothermometer in soil and paleosol carbonate: Geochimica et Cosmochimica Acta, v. 105, p. 92–107, https://doi.org/10.1016/j.gca.2012.11.031
Risi, C., Bony, S., and Vimeux, F., 2008, Influence of convective processes on the isotopic composition (δ^{18}O

and δD) of precipitation and water vapor in the tropics: 2. Physical interpretation of the amount effect: Journal of Geophysical Research: Atmospheres, v. 113, n. D19, https://doi.org/10.1029/2008JD009943

Rowley, D. B., 2007, Stable isotope-based paleoaltimetry: Theory and validation: Reviews in Mineralogy and Geochemistry, v. 66, n. 1, p. 23–52, https://doi.org/10.2138/rmg.2007.66.2

Rowley, D. B., and Currie, B. S., 2006, Palaeo-altimetry of the late Eocene to Miocene Lunpola basin, central Tibet: Nature, v. 439, p. 677–681, https://doi.org/10.1038/nature04506

Rowley, D. B., and Garzione, C. N., 2007, Stable Isotope-Based Paleoaltimetry: Annual Review of Earth and Planetary Sciences, v. 35, p. 463–508, https://doi.org/10.1146/annurev.earth.35.031306.140155

Rowley, D. B., Pierrehumbert, R. T., and Currie, B. S., 2001, A new approach to stable isotope-based paleoaltimetry: Implications for paleoaltimetry and paleohypsometry of the High Himalaya since the Late Miocene: Earth and Planetary Science Letters, v. 188, n. 1–2, p. 253–268, https://doi.org/10.1016/s0012-821x(01)00324-7

Roy, M., MacCarthy, J. K., and Selverstone, J., 2005, Upper mantle structure beneath the eastern Colorado Plateau and Rio Grande rift revealed by Bouguer gravity, seismic velocities, and xenolith data: Geochemistry, Geophysics, Geosystems, v. 6, n. 10, Q10007, https://doi.org/10.1029/2005GC001008

Sahagian, D., Proussevitch, A., and Carlson, W., 2002, Timing of Colorado Plateau uplift: Initial constraints from vesicular basalt-derived paleoelevations: Geology, v. 30, n. 9, p. 807–810, https://doi.org/10.1130/0091-7613(2002)030<0807:TOCPUI>2.0.CO;2

Schauer, A. J., Kelson, J., Saenger, C., and Huntington, K. W., 2016, Choice of ^{17}O correction affects clumped isotope (Δ_{47}) values of CO_2 measured with mass spectrometry: Rapid Communications in Mass Spectrometry, v. 30, n. 24, p. 2607–2616, https://doi.org/10.1002/rcm.7743

Schemmel, F., Mikes, T., Rojay, B., and Mulch, A., 2013, The impact of Topography on isotopes in precipitation across the central Anatolian Plateau (Turkey): American Journal of Science, v. 313, n. 2, p. 61–80, https://doi.org/10.2475/02.2013.01

Seager, W. R., 2004, Laramide (Late Cretaceous-Eocene) tectonics of southwestern New Mexico, *in* Mack, G. M., and Giles, K. A., editors, The geology of New Mexico, A geologic history: New Mexico Geological Society Special Publication 11, p. 183–202.

Seager, W. R., and Mack, G. H., 1986, Laramide paleotectonics of southern New Mexico, *in* Peterson, J. D., editor, Paleotectonics of southern New Mexico: American Association of Petroleum Geologists, Memoir 41, p. 669–685.

Serkan-Arca, M., Kapp, P., and Johnson, R. A., 2010, Cenozoic crustal extension in southeastern Arizona and implications for models of core-complex development: Tectonophysics, v. 488, n. 1–4, p. 174–190, https://doi.org/10.1016/j.tecto.2010.03.021

Sewall, J. O., and Sloan, L. C., 2006, Come a little bit closer: A high-resolution climate study of the early Paleogene Laramide foreland: Geology, v. 34, n. 2, p. 81–84, https://doi.org/10.1130/G22177.1

Sewall, J. O., Sloan, L. C., Huber, M., and Wing, S., 2000, Climate sensitivity to changes in land surface characteristics: Global and Planetary Change, v. 26, n. 4, p. 445–465, https://doi.org/10.1016/S0921-8181(00)00056-4

Shafiqullah, M., Damon, P. E., Lynch, D. J., Kuck, P. H., and Rehrig, W. A., 1978, Mid-Tertiary Magmatism in Southeastern Arizona, *in* Callender, J. F., Wilt, J., Clemons, R. E., and James, H. L., editors, Land of Cochise (Southeastern Arizona): New Mexico, New Mexico Geological Society Guidebook, 29th Annual Field Conference Guidebook, p. 231–241.

Snell, K. E., Koch, P., Druschke, P., Foreman, B., and Eiler, J. M., 2014, High elevation of the 'Nevadaplano' during the Late Cretaceous: Earth and Planetary Science Letters, v. 386, p. 52–63, https://doi.org/10.1016/j.epsl.2013.10.046

Spencer, J. E., 1996, Uplift of the Colorado Plateau due to lithospheric attenuation during Laramide low-angle subduction: Journal of Geophysical Research-Solid Earth, v. 101, n. B6, p. 13595–13609, https://doi.org/10.1029/96JB00818

Thompson, G. A., and Zoback, M. L., 1979, Regional geophysics of the Colorado Plateau: Tectonophysics, v. 61, n. 1–3, p. 149–181, https://doi.org/10.1016/0040-1951(79)90296-8

Tindall, J., Flecker, R., Valdes, P., Schmidt, D. N., Markwick, P., and Harris, J., 2010. Modelling the oxygen isotope distribution of ancient seawater using a coupled ocean–atmosphere GCM: Implications for reconstructing early Eocene climate: Earth and Planetary Science Letters, v. 292, n. 3–4, p. 265–273, https://doi.org/10.1016/j.epsl.2009.12.049

Van Wijk, J. W., Baldridge, W. S., Van Hunen, J., Goes, S., Aster, R., Coblentz, D. D., Grand, S. P., and Ni, J., 2010, Small-scale convection at the edge of the Colorado Plateau: Implications for topography, magmatism, and evolution of Proterozoic lithosphere: Geology, v. 38, n. 7, p. 611–614, https://doi.org/10.1130/G31031.1

Walsh, S. L., Prothero, D. R., and Lundquist, D. J., 1996, Stratigraphy and paleomagnetism of the middle Eocene Friars Formation and Poway Group, southwestern San Diego County, California, *in* Prothero, D. R., and Emry, R. J., editors, The Terrestrial Eocene-Oligocene Transition in North America: Cambridge, Cambridge University Press, p. 120–154, https://doi.org/10.1017/cbo9780511665431.007

Western Regional Climatic Center 2015, http://www.wrcc.dri.edu/

Wright, W. E., ms, 2001, Delta-deuterium and delta-oxygen-18 in mixed conifer system in the United States southwest: The potential of delta-oxygen-18 in *Pinus ponderosa* tree rings as a natural environmental recorder: Tucson, Arizona, University of Arizona, Ph. D. dissertation, 328 p.

Wright, W. E., Long, A., Comrie, A. C., Leavitt, S. W., Cavazos, T., and Eastoe, C., 2001, Monsoonal moisture sources revealed using temperature, precipitation, and precipitation stable isotope timeseries: Geophysical Research Letters, v. 28, n. 5, p. 787–790, https://doi.org/10.1029/2000GL012094

Zandt, G., Gilbert, H., Owens, T. J., Ducea, M., Saleeby J., and Jones, C. H., 2004, Active foundering of a continental arc root beneath the southern Sierra Nevada in California: Nature, v. 431, p. 41–46, https://doi.org/10.1038/nature02847